

# Ranging-Based Localizability Optimization for Mobile Robotic Networks

Justin Cano, *Member, IEEE*, and Jerome Le Ny, *Senior Member, IEEE*

**Abstract**—In robotic networks relying on noisy range measurements between agents for cooperative localization, the achievable positioning accuracy strongly depends on the network geometry. This motivates the problem of planning robot trajectories in such multi-robot systems in a way that maintains high localization accuracy. We present potential-based planning methods, where localizability potentials are introduced to characterize the quality of the network geometry for cooperative position estimation. These potentials are based on Cramér Rao Lower Bounds (CRLB) and provide a theoretical lower bound on the error covariance achievable by any unbiased position estimator. In the process, we establish connections between CRLBs and the theory of graph rigidity, which has been previously used to plan the motion of robotic networks. We develop decentralized deployment algorithms appropriate for large networks, and we use equality-constrained CRLBs to extend the concept of localizability to scenarios where additional information about the relative positions of the ranging sensors is known. We illustrate the resulting robot deployment methodology through simulated examples and an experiment.

**Index Terms**—Multi-robot systems, Path planning, Cooperative localization

## I. INTRODUCTION

MOBILE robots require accurate, computationally efficient and low power localization systems to navigate their environment and perform their assigned tasks. Positioning can rely on various technologies, e.g., wheel odometry, computer vision or long- and short-range radio frequency (RF) systems, each with distinct advantages and drawbacks, depending on the environment and requirements. For example, the most common methods of terrestrial localization rely on RF signals from Global Navigation Satellite Systems (GNSS) to achieve meter- to centimeter-level accuracy, but these systems do not operate indoors or when the line of sight to the satellites is obstructed, and are sensitive to interference.

Multiple robots can collaborate to improve the accuracy and coverage of their individual localization solution [3], [4]. In particular, they can leverage information about their proximity to other location-aware nodes [3] or use relative position [4], bearing [5] or distance measurements [6], [7] between them to estimate their individual positions in a common reference frame. Relative bearing measurements can be provided by monocular cameras for example, range measurements by short-range RF systems, and relative position

measurements by LiDARs or stereo cameras. In this paper, we focus on collaborative localization in Multi-Robot Systems (MRS) *using only range measurements*. This is motivated by the fact that accurate distance measurements can be deduced from Time-of-Flight (ToF) measurements obtained from inexpensive short-range RF communication systems, e.g., Ultra-Wide Band (UWB) transceivers [8]–[10]. In particular, such systems associate distance measurements unambiguously with pairs of robots, simply by having the robots broadcast their IDs.

Once the robots have measured their relative distances, many algorithms exist to compute from these measurements an estimate of the robot positions, see, e.g., [11] for a recent survey. These algorithms can be centralized or decentralized, applicable to static or mobile networks, appropriate or not for real-time localization, etc. Two major factors determine the ability of these algorithms to solve the position estimation problem and their accuracy. First, enough relative distance measurements should be available, which links the feasibility of the location estimation problem to the concept of *rigidity* [12]–[14] of the *ranging graph* corresponding to these measurements. Second, satisfying the graph-theoretic condition of rigidity is still insufficient to guarantee accurate localization of the individual agents, when measurement noise is inevitably present. For example, a group of robots that are almost aligned can form a rigid formation if enough range measurements are available, but can only achieve poor localization accuracy in practice. Indeed, the spatial *geometry* of the network strongly influences the accuracy of position estimates in the presence of measurement noise [15], a phenomenon known as Dilution of Precision (DOP) in the navigation literature [16, Chap. 7]. We call here *localizability* the ability to accurately estimate the positions of the individual robots of an MRS in a given geometric configuration, using relative measurements.

In contrast to static sensor networks or GNSS, an MRS can actively adjust its geometry, e.g., some of the robot positions and orientations, in order to improve its overall localizability. This results in a coupling between the motion planning and localization problem for the group. Maintaining the rigidity of the ranging graph during the motion of an MRS is a stronger condition than maintaining its connectivity, but similar techniques can be used to address both problems. In particular, we can capture the degree of connectivity or rigidity of the graph using a function of the first non-zero eigenvalue of a type of Laplacian matrix, and guide the MRS along paths or configure its nodes in ways that increase this function. This is the approach adopted for example in [17]–[19] for improving connectivity and in [20]–[23] for improving rigidity.

This work was supported by FRQNT under grant 2018-PR-253646 and by NSERC under grant RGPIN-5287-2018.

The authors are with the Department of Electrical Engineering, Polytechnique Montreal, and with GERAD, Montreal, QC H3T 1J4, Canada {justin.cano, jerome.le-ny}@polymtl.ca.

Preliminary versions of this paper appeared in [1] and [2].

This article builds on this principle to optimize localizability. Following an approach that we initially proposed in [1], [2], we leverage Cramér Rao Lower Bounds (CRLBs) [24, Chap. 14] to construct localizability potentials, which can then be used as artificial potentials [25] to drive the motion of an MRS toward geometric configurations promoting good localization.

The CRLB provides a lower bound on the covariance of any unbiased position estimate constructed from the relative range measurements available in the robot network. Tighter covariance lower bounds exist, such as Barankin bounds [26], but an advantage of the CRLB is that it is relatively easy to compute and admits a closed-form expression for the problem considered here, assuming Gaussian noise [15]. Moreover, as we show in Section IV, the CRLB for Gaussian noise is in fact closely related to the so-called *rigidity matrix* of the ranging graph. This does not come as a surprise, since the Gaussian CRLB is known to correspond to DOP expressions for least-squares estimators, which are implicitly derived in [20] for example and also linked to the rigidity matrix. The CRLB only provides a lower bound on estimation performance and there is generally no guarantee that a position estimator actually achieves it. Nonetheless, using this bound as a proxy to optimize sensor placement is a well accepted approach [27]. An important advantage of this approach is that the motion planning strategy becomes independent of the choice of position estimator implemented in the network.

**Contributions:** First, this paper formulates a novel motion planning problem allowing an MRS to optimize its localizability, by minimizing appropriate cost functions based on the Fisher Information Matrix (FIM) appearing in the CRLB. Second, we establish an explicit connection between localizability and the weighted rigidity matrices introduced in [22], [23]. One of the benefits of establishing this connection is to see that various artificial potentials can be constructed from the FIM to capture localizability, as discussed in the literature on optimal experimental design [28] or optimal sensing with mobile robots, see, e.g., [27], [29], [30]. Some of these functions may be more conveniently optimized than the smallest nonzero eigenvalue, which is the standard potential used for connectivity and rigidity maintenance. Third, by leveraging the structure of the FIM matrix, we propose new distributed algorithms enabling the deployment of groups of robots carrying ranging sensors in a scalable and robust manner. Fourth, we extend the results to robots carrying multiple ranging sensors, using the theory of *constrained* CRLBs [31] to account for the presence of additional rigidity constraints. This can be viewed as an alternative and simpler approach to deriving intrinsic CRLBs on the manifold of rigid motions [32], [33].

The structure of the paper is as follows. First, we define the deployment problem in Section II, including localizability potentials further discussed in Section III. Then, we derive in Section IV the closed-form expression for the FIM and analyze its structure, which allows us to introduce in Section V decentralized methods to estimate the gradients of the localizability potentials. Section VI extends the analysis to the case of robots carrying multiple ranging sensors. The deployment algorithms are validated in two simulated scenarios in Section VII, and experimental results using RF range measurements

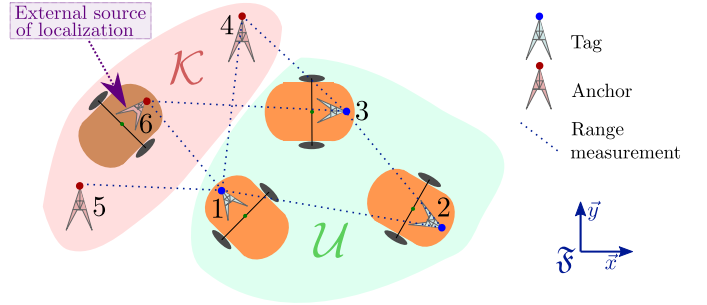


Fig. 1: Illustration of the setup in 2D with 3 mobile tags and 3 anchors, 2 of whom are fixed. The links for the ranging pairs are shown. The ranging graph includes 3 additional implicit links between the anchors, not shown.

from UWB transceivers are described in Section VIII.

This article builds on the conference paper [1], which introduced the concept of localizability potentials for the deployment of MRS in two dimensions. Here we extend the methodology to three dimensions, introduce new distributed optimization schemes, discuss useful properties on the FIM and make a clearer connection with rigidity theory. We also generalize the conference paper [2], which considered robots carrying multiple sensors, by developing the results in three dimensions and integrating the full relative position information in the CRLB rather than just relative distances, which is significantly more challenging. We demonstrate in simulation the improvement achievable with this extension.

**Notation:** We write vectors and matrices with a bold font. The all-one vector of size  $p$  is denoted  $\mathbf{1}_p$ . The notation  $\mathbf{x} = \text{col}(\mathbf{x}_1, \dots, \mathbf{x}_n)$  means that the vectors or matrices  $\mathbf{x}_i$  are stacked on top of each other, and  $\text{diag}(\mathbf{A}_1, \dots, \mathbf{A}_k)$  denotes a block diagonal matrix with the matrices  $\mathbf{A}_i$  on the diagonal. The nullspace of a matrix  $\mathbf{A}$  is denoted  $\ker \mathbf{A}$ . For  $\mathbf{A}$  and  $\mathbf{B}$  symmetric matrices of the same dimensions,  $\mathbf{A} \succeq \mathbf{B}$  means that  $\mathbf{A} - \mathbf{B}$  is positive semidefinite and  $\mathbf{A} \succ \mathbf{B}$  that it is positive definite. If  $\mathbf{A}$  is a symmetric matrix,  $\lambda_{\min}(\mathbf{A})$  and  $\lambda_{\max}(\mathbf{A})$  denote its minimum and maximum eigenvalues. The time derivative of a vector-valued function  $t \mapsto \mathbf{x}(t)$  is denoted  $\dot{\mathbf{x}}$ . The expectation of a random vector  $\mathbf{x}$  is denoted  $\mathbb{E}[\mathbf{x}]$  and its covariance matrix  $\text{cov}[\mathbf{x}] = \mathbb{E}[(\mathbf{x} - \mathbb{E}[\mathbf{x}])(\mathbf{x} - \mathbb{E}[\mathbf{x}])^T]$ . For a differentiable function  $f : \mathbb{R}^p \rightarrow \mathbb{R}^q$ ,  $\frac{\partial f(\mathbf{p})}{\partial \mathbf{p}}$  represents the  $q \times p$  Jacobian matrix of  $f$ , with components  $\partial f_i(\mathbf{p}) / \partial p_j$  for  $1 \leq i \leq q$ ,  $1 \leq j \leq p$ . When  $q = 1$ ,  $\partial^2 f(\mathbf{p}) / \partial \mathbf{p} \partial \mathbf{p}^T$  denotes the Hessian, i.e., the square matrix with components  $\partial^2 f(\mathbf{p}) / \partial p_i \partial p_j$ . Finally,  $\mathbf{1}_e$  is equal to 1 if the logical expression  $e$  is true and 0 otherwise, and for a set  $\mathcal{S}$  we also use the alternative notation  $\mathbf{1}_{\mathcal{S}}(i) := \mathbf{1}_{i \in \mathcal{S}}$ .

## II. PROBLEM STATEMENT

Consider a set of  $N$  nodes in the  $n$ -dimensional Euclidean space, where  $n = 2$  or  $n = 3$ . We fix a global reference frame denoted  $\mathfrak{F} = (O, \vec{x}, \vec{y}, \vec{z})$  if  $n = 3$  or  $\mathfrak{F} = (O, \vec{x}, \vec{y})$  if  $n = 2$ . For  $1 \leq i \leq N$ , we write the coordinates of node  $i$  in that frame  $\mathbf{p}_i := [x_i, y_i, z_i]^T$  if  $n = 3$  or  $\mathbf{p}_i := [x_i, y_i]^T$  if  $n = 2$ , and we let  $\mathbf{p} := \text{col}(\mathbf{p}_1, \dots, \mathbf{p}_N) \in \mathbb{R}^{nN}$  denote the global spatial configuration of the nodes, which can vary with time.

As illustrated on Fig. 1, some of these nodes are carried by mobile robots, while others could remain at fixed locations. We suppose that the coordinates of a subset  $\mathfrak{K}$  of the nodes are perfectly known in  $\mathfrak{F}$ , for  $1 < |\mathfrak{K}| := K < N$ , and refer to these nodes as *anchors*. The anchors could be placed at fixed locations or they could be mobile, as long as we can precisely localize them via external means, e.g., using accurate GNSS receivers. The other nodes, also mobile or fixed and whose positions are unknown and need to be estimated, are called *tags* in the following. They form a set denoted  $\mathcal{U}$ , with  $|\mathcal{U}| := U = N - K$ .

Next, we assume that  $P$  pairs of nodes, called ranging pairs, can measure their distance (with each such pair containing at least one tag). For a ranging pair of nodes  $(i, j)$ , we denote  $d_{ij}$  the true distance between the nodes and  $\tilde{d}_{ij}$  a corresponding measurement, to which both nodes  $i$  and  $j$  have access. In the following, we consider measurement models assuming either additive Gaussian noise

$$\tilde{d}_{ij} = d_{ij} + \nu_{ij}, \quad \nu_{ij} \sim \mathcal{N}(0, \sigma^2), \quad (1)$$

or multiplicative log-normal noise

$$\tilde{d}_{ij} = d_{ij} e^{\mu_{ij}}, \quad \mu_{ij} \sim \mathcal{N}(0, \bar{\sigma}^2), \quad (2)$$

where the noise realizations  $\nu_{ij}$  or  $\mu_{ij}$  are independent for all  $i, j$  and  $\sigma^2, \bar{\sigma}^2 \in \mathbb{R}^+$  are given covariances. We collect all the measured distances  $\tilde{d}_{ij}$  at a given time in the vector  $\tilde{\mathbf{d}} = [\dots, \tilde{d}_{ij}, \dots]^T \in \mathbb{R}^P$ . We also define an undirected graph  $\mathcal{G} = (\mathcal{E}, \mathcal{V})$ , called the *ranging graph*, whose vertices  $\mathcal{V}$  are the  $N$  nodes and with an edge in  $\mathcal{E}$  for each ranging pair and for each pair of anchors. In particular, the subgraph of  $\mathcal{G}$  formed by the anchors is a complete graph, which is consistent with the fact that the distances between anchors are implicitly known from their coordinates. Two nodes linked by an edge in  $\mathcal{G}$  are called neighbors and we denote by  $\mathcal{N}_i$  the set of neighbors of  $i$  or *neighborhood* of  $i$ , for  $1 \leq i \leq N$ . Let  $E = P + \frac{K(K-1)}{2}$  be the total number of edges in  $\mathcal{G}$ .

A concrete implementation of the previous system is as follows. The nodes could correspond to RF transceivers capable of measuring their distance with respect to other nodes within their communication radius. Radiolocation protocols such as Two-Way Ranging (TWR), Time of Arrival (ToA) or Time Difference of Arrival (TDoA) [8], [34] use the timestamps of messages exchanged by the transceivers to estimate the ToF of these messages and deduce distance measurements, which can be assumed to be of the form (1), at least under line-of-sight signal propagation conditions. Another ranging method consists in measuring the strength of a received signal (RSS) to deduce the distance to the transmitter using a path loss propagation model [34]. This method typically leads to a distance measurement model of the form (2), assuming again a simple radio propagation environment [15], [35].

We assume that the nodes implement a cooperative localization scheme, in order to jointly produce an estimate  $\hat{\mathbf{p}}$  of all their coordinates  $\mathbf{p}$  in  $\mathfrak{F}$ , based on the noisy measurements  $\tilde{\mathbf{d}}$  and the knowledge of the anchor coordinates. As we explain in Section III, the value of  $\mathbf{p}$  itself strongly influences the achievable accuracy of its estimate. Hence, we introduce in that section some real-valued functions  $J_{\text{loc}} : \mathbb{R}^{nN} \rightarrow \mathbb{R}$  that

can serve as *localizability potentials*, i.e., such that a low value (resp. high value) for  $J_{\text{loc}}(\mathbf{p})$  means that the performance of an estimator at configuration  $\mathbf{p}$  is expected to be good (resp. bad). A localizability potential can then serve as an artificial potential for motion planning [25], to guide or constrain the motion of an MRS to configurations that are favorable for accurate cooperative localization. Concretely, consider a potential function  $J(\mathbf{p}) = \alpha J_1(\mathbf{p}) + (1 - \alpha) J_{\text{loc}}(\mathbf{p})$ , for  $\alpha \in (0, 1)$ , where  $J_1$  may include attractive and repulsive potentials to steer robots toward desired locations [36] and away from obstacles [25], to maintain network connectivity [19], to cover an area [37], etc. One can then generate a sequence of configurations  $\mathbf{p}(0), \mathbf{p}(1), \dots$ , for the MRS by following the gradient descent scheme

$$\mathbf{p}_{i,k+1} = \mathbf{p}_{i,k} - \gamma_k \left( \frac{\partial J(\mathbf{p}_k)}{\partial \mathbf{p}_i} \right)^T, \quad (3)$$

for each mobile node  $i$ , with  $\{\gamma_k\}_{k \geq 0}$  a sequence of appropriate stepsizes. The presence of  $J_{\text{loc}}$  in the overall potential favours configurations that have higher localizability, and this effect becomes more pronounced as  $\alpha$  increases. Alternatively, one can also minimize  $J_1$  subject to a constraint on the maximum tolerable value of  $J_{\text{loc}}$ . Note however that as in most cases where artificial potentials are used to plan the motion of an MRS, the gradient descent scheme (3) typically only leads to locally optimal configurations.

A key issue when relying on artificial potentials to provide goal configurations to an MRS is to ensure that each mobile node  $i$  can compute the gradient  $(\partial J_{\text{loc}}(\mathbf{p}(k))/\partial \mathbf{p}_i)^T$  with respect to its coordinates in (3) by exchanging information only with its immediate neighbors in the communication network, *which we assume here to coincide with the ranging graph* (although in general the anchors will not need to communicate with each other). This ensures scalability to large networks and improves the robustness of the network against the loss of nodes. The design of distributed gradient descent schemes for the localizability potentials is discussed in Section V.

In summary, the problem considered in this paper is to first define appropriate functions that can serve as localizability potentials and then design distributed gradient descent algorithms for these potentials in order to deploy an MRS with ranging sensors while ensuring that its cooperative localization scheme remains precise. In addition, we show in Section VI how to adapt the definition of the localizability potentials and the gradient descent scheme to a more complex situation where multiple tags can be carried by the same robot. This introduces additional constraints on the positions  $\mathbf{p}$ , which should be taken into account by localization and motion planning algorithms. These constraints can be used in practice to provide more accurate full pose estimates for the robots.

**Remark 1.** *In practice, the tags have access to their position  $\mathbf{p}$  only through their estimates  $\hat{\mathbf{p}}$ . As a result, when using artificial potentials for motion planning, the gradient descent scheme (3) cannot be directly implemented, and the standard approach is to compute and follow the gradient at the current estimate, i.e., use  $\partial J(\hat{\mathbf{p}}_k)/\partial \mathbf{p}_i$  in (3). Since including a localizability potential aims to improve the accuracy of the*

position estimates along the robots' paths, it contributes to making this approximation of ignoring position uncertainty less problematic. Alternatively, (3) can also be used to compute a sequence of steps, i.e., plan a future trajectory for the MRS, in which case we assume at the planning stage that the agents will be able to track that trajectory perfectly. Moreover, we empirically study the behavior of the scheme (3) with gradients evaluated at the imperfect position estimates, both in simulations in Section VII and through experiments in Section VIII. In particular, our experiment confirms the intuitive fact that enhancing the localizability is important to ensure that the robots are able to reliably follow their desired trajectories.

**Remark 2.** In general, the ranging graph  $\mathcal{G}$  could change over time as nodes move in their environment. In this case, the algorithms presented later could still be implemented at each period over the current ranging graph, but localizability could become poor if critical ranging pairs become disconnected. To address this issue, ranging between specific pairs can be maintained by adding connectivity potentials to the function  $J_1$  above. Alternatively, when we use the model (2) or alternative models where the variance degrades with distance [38], then  $J_{loc}$  increases when the links become longer, a consequence of the result (5) stated in the next section. Hence, in a manner similar to the use weighted graph models for connectivity [17] and rigidity [22], maintaining ranging distance between nodes can be promoted directly through the localizability potential.

### III. LOCALIZABILITY POTENTIALS

This section is concerned with defining artificial potentials that can be used as localizability potentials. The proposed definitions require that we first recall some notions from estimation theory related to the CRLB.

#### A. Constrained Cramér-Rao Lower Bound

We assume that the position estimator implemented by the MRS is unbiased, i.e., satisfies  $\mathbb{E}[\hat{\mathbf{p}}] = \mathbf{p}$ . We then focus on finding configurations  $\mathbf{p}$  for which the error covariance matrix  $\mathbb{E}[(\hat{\mathbf{p}} - \mathbf{p})(\hat{\mathbf{p}} - \mathbf{p})^\top]$  for  $\hat{\mathbf{p}}$ , which is then also the covariance matrix  $\text{cov}[\hat{\mathbf{p}}]$ , is "small" in some sense. More precisely, since the error covariance depends on the specific estimator used and can be difficult to predict analytically, we use the CRLB, a lower bound on the covariance of any unbiased estimator, to quantify the quality of a configuration  $\mathbf{p}$ . Although this implicitly assumes that an estimator can be constructed to achieve or approach this lower bound, this methodology is commonly used in optimal experiment design and sensor placement [27], [28]. In general, the CRLB corresponds to the inverse of the Fisher Information Matrix (FIM), which we define below.

**Definition 1 (FIM).** Let  $\mathbf{x} \in \mathbb{R}^p$  be a deterministic parameter vector and  $\mathbf{y} \in \mathbb{R}^q$  a random observation vector, for some positive integers  $p, q$ . Define  $f : \mathbb{R}^q \times \mathbb{R}^p \rightarrow \mathbb{R}^+$  the Probability Density Function (PDF) of  $\mathbf{y}$ , which depends on the parameter  $\mathbf{x}$ , so that we write  $f(\mathbf{y}; \mathbf{x})$ . Under some

regularity assumptions on  $f$  (see [24, Chap. 14]), the  $p \times p$  Fisher Information Matrix (FIM) of this PDF is defined as

$$\mathbf{F}(\mathbf{x}) = -\mathbb{E}_{\mathbf{y}} \left[ \frac{\partial^2 \ln f(\mathbf{y}; \mathbf{x})}{\partial \mathbf{x} \partial \mathbf{x}^\top} \right]. \quad (4)$$

The matrix  $\mathbf{F}(\mathbf{x})$  is symmetric and positive semi-definite.

In the position estimation problem, the parameters of interest are the node coordinates in the vector  $\mathbf{p} \in \mathbb{R}^{nN}$ , whereas the random observations are contained in the vector  $\tilde{\mathbf{d}}$ . As computed in [15], the FIM of the PDF  $f(\tilde{\mathbf{d}}; \mathbf{p})$  is an  $nN \times nN$  matrix that depends on  $\mathbf{p}$  and can be decomposed into  $n \times n$  blocks  $\mathbf{F}_{ij}$  such that

$$\begin{aligned} \mathbf{F}_{ij}(\mathbf{p}) &= \mathbf{F}_{ij}(\mathbf{p}_{ij}) = -\frac{1}{d_{ij}^{2\kappa} \sigma^2} \mathbf{p}_{ij} \mathbf{p}_{ij}^\top \mathbf{1}_{\mathcal{N}_i}(j), \text{ if } i \neq j, \\ \mathbf{F}_{ii}(\mathbf{p}) &= -\sum_{j \neq i} \mathbf{F}_{ij}, \end{aligned} \quad (5)$$

where  $\mathbf{p}_{ij} := \mathbf{p}_i - \mathbf{p}_j$ , and  $\kappa = 1$  for the additive noise model (1) or  $\kappa = 2$  for the multiplicative noise model (2). The result (5) can be obtained using the Slepian-Bangs formula [39, Section 3.9] or by direct calculation.

Note however that estimating the anchor positions is not needed, since the locations of these nodes are known. The fact that  $\hat{\mathbf{p}}_i := \mathbf{p}_i$  for all  $i \in \mathcal{K}$ , with  $\mathbf{p}_i$  known, should be taken into account by an estimator of the tag positions, and hence should also be taken into account when bounding the covariance of these estimators. We can rely on the theory of CRLBs with equality constraints on the estimated parameters in order to include these trivial constraints on the anchor positions and later in Section VI also additional rigid constraints on the tag positions.

**Theorem 1** (Equality constrained CRLB [31]). Let  $\mathbf{x} \in \mathbb{R}^p$  be a deterministic parameter vector and  $\mathbf{y} \in \mathbb{R}^q$  a random observation vector, for some positive integers  $p, q$ . Let  $\mathbf{h} : \mathbb{R}^p \rightarrow \mathbb{R}^c$ , for  $c \leq p$ , be a differentiable function such that  $\mathbf{h}(\mathbf{x}) = \mathbf{0}$ . Let  $\hat{\mathbf{x}}$  be an unbiased estimate of  $\mathbf{x}$  also satisfying  $\mathbf{h}(\hat{\mathbf{x}}) = \mathbf{0}$  and with finite covariance matrix. Define  $\mathbf{F}_c := \mathbf{A}^\top \mathbf{F} \mathbf{A}$ , the constrained Fisher Information Matrix, where  $\mathbf{A}$  is any matrix whose columns span  $\ker \frac{\partial \mathbf{h}}{\partial \mathbf{x}}$ , and  $\mathbf{F}$  is the FIM defined in (4). Then, the following inequality holds

$$\text{cov}[\hat{\mathbf{x}}] \succeq \mathbf{A} (\mathbf{F}_c)^\dagger \mathbf{A}^\top =: \mathbf{B}_c \quad (6)$$

where  $\dagger$  denotes the Moore-Penrose pseudo-inverse [40, p. 21].

Consider now the problem of estimating the vector of tag coordinates  $\mathbf{p}_U \in \mathbb{R}^{nU}$  based on the distance measurements  $\tilde{\mathbf{d}}$  and knowledge of the anchor coordinates  $\mathbf{p}_\mathcal{K} \in \mathbb{R}^{nK}$ . Order the nodes so that  $\mathbf{p} = \text{col}(\mathbf{p}_U, \mathbf{p}_\mathcal{K})$ , and partition the FIM defined in (5) accordingly as

$$\mathbf{F} = \begin{bmatrix} \mathbf{F}_U & \mathbf{F}_{U\mathcal{K}} \\ \mathbf{F}_{U\mathcal{K}}^\top & \mathbf{F}_\mathcal{K} \end{bmatrix}, \quad (7)$$

with in particular  $\mathbf{F}_U$  a symmetric positive semi-definite matrix of size  $nU \times nU$ . We then have the following result.

**Proposition 1.** Let  $\hat{\mathbf{p}}_{\mathcal{U}}$  be an unbiased estimate of the tag positions  $\mathbf{p}_{\mathcal{U}}$ , based on the measurements  $\tilde{\mathbf{d}}$  and the knowledge of the anchor positions  $\mathbf{p}_{\mathcal{K}}$ . Then

$$\text{cov}[\hat{\mathbf{p}}_{\mathcal{U}}] \succeq \mathbf{F}_{\mathcal{U}}^{\dagger}(\mathbf{p}). \quad (8)$$

*Proof.* This result is a corollary of Proposition 5 stated below, with  $\mathbf{f}_c \equiv \mathbf{0}$  in (28) and so  $\mathbf{A}_{\mathcal{U}} = \mathbf{I}_{n_{\mathcal{U}}}$ .  $\square$

### B. Localizability Potentials and Optimal Design

Given (8), the following functions are possible candidates to define potential functions that penalize configurations of the ranging network leading to poor localizability

$$J_A(\mathbf{p}) = \text{Tr} \{ \mathbf{F}_{\mathcal{U}}^{-1}(\mathbf{p}) \} \quad (\text{A-Optimal Design}), \quad (9)$$

$$J_D(\mathbf{p}) = -\ln \det \{ \mathbf{F}_{\mathcal{U}}(\mathbf{p}) \} \quad (\text{D-Optimal Design}), \quad (10)$$

$$J_E(\mathbf{p}) = -\lambda_{\min} \{ \mathbf{F}_{\mathcal{U}}(\mathbf{p}) \} \quad (\text{E-Optimal Design}), \quad (11)$$

assuming in the first two cases that  $\mathbf{F}_{\mathcal{U}}(\mathbf{p})$  is invertible. In the following, we refer to the functions  $J_A$ ,  $J_D$  and  $J_E$  as the A-Opt, D-Opt and E-Opt potentials respectively, using standard terminology from optimal experiment design [28].

In each case, configurations  $\mathbf{p}$  for which  $J(\mathbf{p})$  takes large values correspond to geometries for which the error covariance matrix of an unbiased position estimator will necessarily be “large” in a sense defined by the choice of potential. Hence, for (9), we have from (8) that  $J_A(\mathbf{p})$  is a lower bound on  $\text{Tr} \{ \text{cov}[\hat{\mathbf{p}}_{\mathcal{U}}] \}$ , which represents the total mean-squared error (MSE) of the unbiased estimator  $\hat{\mathbf{p}}_{\mathcal{U}}$ . Similarly, (10) corresponds to a lower bound on  $\ln \det(\text{cov}[\hat{\mathbf{p}}_{\mathcal{U}}])$ , which would be equal (up to a constant) to the statistical entropy of  $\hat{\mathbf{p}}_{\mathcal{U}}$ , if this estimate were to follow a normal distribution. Finally, still assuming  $\mathbf{F}_{\mathcal{U}} \succ 0$ , minimizing  $J_E$  in (11) aims to minimize the maximum eigenvalue of  $\mathbf{F}_{\mathcal{U}}^{-1}$  (equal to  $1/\lambda_{\min}(\mathbf{F}_{\mathcal{U}})$ ), which is a lower bound on the maximum eigenvalue or induced 2-norm of  $\text{cov}[\hat{\mathbf{p}}_{\mathcal{U}}]$ . Potentials like  $J_E$  are often used to maintain the connectivity [17]–[19] or rigidity [22], [23] of an MRS, which are closely related problems.

Once a potential has been chosen, it can be used to move the nodes to configurations of low potential values, where the localization accuracy is expected to be high. This can be done for example by descending the gradient of the potential, as discussed in Sections V and VI.

**Remark 3.** Another a priori possible potential is

$$J_T(\mathbf{p}) = -\text{Tr} \{ \mathbf{F}_{\mathcal{U}}(\mathbf{p}) \}.$$

Configurations  $\mathbf{p}$  that minimize this potential are called *T-optimal designs* [28]. However, in our case we can compute

$$J_T(\mathbf{p}) = -\alpha \sum_{\{i,j\} \in \mathcal{E}} d_{ij}^{2-2\kappa},$$

with  $\alpha$  a positive constant. In the case of additive Gaussian noise (1),  $\kappa = 1$  and  $J_T$  is constant, so that it cannot be used to optimize  $\mathbf{p}$ . In the case of multiplicative noise (2), we have  $\kappa = 2$  so  $J_T(\mathbf{p}) = -\alpha \sum_{\{i,j\} \in \mathcal{E}} d_{ij}^{-2}$  becomes a simple attractive potential. In this case,  $J_T$  cannot be used alone as a potential, since its global minimum is trivially achieved when all agents occupy the same position. In view of these remarks,  $J_T$  is not considered further in the following.

## IV. PROPERTIES OF THE FISHER INFORMATION MATRIX

In this section, we study certain algebraic properties of the FIM that are useful for the design of algorithms in the next sections. In particular, we establish connections between the FIM and rigidity theory.

### A. Infinitesimal Rigidity

For the ranging graph  $\mathcal{G} = (\mathcal{E}, \mathcal{V})$ , the incidence matrix  $\mathbf{H} \in \mathbb{Z}^{E \times N}$  is defined by first assigning an arbitrary direction  $i \rightarrow j$  to each edge  $\{i, j\}$  of  $\mathcal{E}$ , and then setting each element as follows:

$$\text{for } \{i, j\} \in \mathcal{E}, k \in \mathcal{V}, H_{i \rightarrow j, k} = \begin{cases} 1 & \text{if } k = i, \\ -1 & \text{if } k = j, \\ 0 & \text{otherwise.} \end{cases}$$

We use throughout the paper the lexicographic ordering to order the edges  $i \rightarrow j$  and hence the rows of  $\mathbf{H}$ . As a result, the rows of  $\mathbf{H}$  corresponding to pairs of tags (in  $\mathcal{U} \times \mathcal{U}$ ) appear first, followed by pairs in  $\mathcal{U} \times \mathcal{K}$  and finally by pairs of anchors, in  $\mathcal{K} \times \mathcal{K}$ .

**Remark 4.** Some references define  $\mathbf{H}$  as an  $N \times E$  matrix, transposing the  $E \times N$  matrix above. Our choice of convention is motivated by the fact that it makes the connection to the rigidity matrix and the FIM clearer below.

Given a ranging graph  $\mathcal{G}$ , a *framework* is a pair  $(\mathcal{G}, \mathbf{p})$ , where the vector  $\mathbf{p} \in \mathbb{R}^{nN}$  contains the positions of all agents. The *rigidity function*  $\mathbf{r} : \mathbb{R}^{nN} \rightarrow \mathbb{R}^E$  of a framework  $(\mathcal{G}, \mathbf{p})$  is defined componentwise by

$$[\mathbf{r}(\mathcal{G}, \mathbf{p})]_{i \rightarrow j} = \frac{1}{2} \|\mathbf{p}_{ij}\|^2, \quad \forall \{i, j\} \in \mathcal{E}, \quad (12)$$

and its *rigidity matrix*  $\mathbf{R}(\mathcal{G}, \mathbf{p}) \in \mathbb{R}^{E \times nN}$  is the Jacobian  $\partial \mathbf{r} / \partial \mathbf{p}$  of the rigidity function [12], [22], which can be written explicitly as

$$\mathbf{R}(\mathcal{G}, \mathbf{p}) = \text{diag}(\dots, \mathbf{p}_{ij}^T, \dots) [\mathbf{H} \otimes \mathbf{I}_n]. \quad (13)$$

In other words, the row  $i \rightarrow j$  of  $\mathbf{R}(\mathcal{G}, \mathbf{p})$  is

$$[0 \quad \dots \quad 0 \quad \mathbf{p}_{ij}^T \quad 0 \quad \dots \quad 0 \quad -\mathbf{p}_{ij}^T \quad 0 \quad \dots \quad 0]$$

with  $\mathbf{p}_{ij}^T$  occupying the  $i^{\text{th}}$  block of  $n$  coordinates and  $-\mathbf{p}_{ij}^T$  the  $j^{\text{th}}$  block. Next, when the node positions vary with time, consider motions that do not change the distances between nodes in ranging pairs, in other words, motions that keep the rigidity function constant. These motions must then satisfy

$$\frac{d\mathbf{r}(\mathcal{G}, \mathbf{p})}{dt} = \mathbf{R}(\mathcal{G}, \mathbf{p}) \frac{d\mathbf{p}}{dt} = \mathbf{0},$$

i.e., the corresponding velocity vectors  $d\mathbf{p}/dt$  must lie in the kernel of  $\mathbf{R}(\mathcal{G}, \mathbf{p})$ . This constraint is rewritten more explicitly in the following definition.

**Definition 2** (Infinitesimal motion of a framework). An *infinitesimal motion* of a framework  $(\mathcal{G}, \mathbf{p})$  is any vector  $\mathbf{v} = \text{col}(\mathbf{v}_1, \dots, \mathbf{v}_N)$  in  $\mathbb{R}^{nN}$ , such that  $\mathbf{v} \in \ker \mathbf{R}(\mathcal{G}, \mathbf{p})$ . Equivalently, for each edge  $\{i, j\} \in \mathcal{E}$ , we have  $\mathbf{p}_{ij}^T(\mathbf{v}_i - \mathbf{v}_j) = \mathbf{0}$ .

Any framework admits a basic set of infinitesimal motions, namely, the *Euclidean* infinitesimal motions of the framework [12], [41], which can be defined for  $n = 3$  as

$$\text{Eucl}_{\mathbf{p}}^3 = \left\{ \text{col}(\mathbf{v} + \boldsymbol{\omega} \times \mathbf{p}_1, \dots, \mathbf{v} + \boldsymbol{\omega} \times \mathbf{p}_N) \mid \mathbf{v}, \boldsymbol{\omega} \in \mathbb{R}^3 \right\},$$

and for  $n = 2$ , with the notation  $\mathbf{p}_i = [x_i, y_i]^T$ ,

$$\text{Eucl}_{\mathbf{p}}^2 = \left\{ \text{col} \left( \mathbf{v} + \boldsymbol{\omega} \begin{bmatrix} y_1 \\ -x_1 \end{bmatrix}, \dots, \mathbf{v} + \boldsymbol{\omega} \begin{bmatrix} y_N \\ -x_N \end{bmatrix} \right) \mid \mathbf{v} \in \mathbb{R}^2, \boldsymbol{\omega} \in \mathbb{R} \right\}.$$

These infinitesimal motions correspond to the global rigid translations and rotations of the whole framework, and it is immediate to verify that the subspace  $\text{Eucl}_{\mathbf{p}}$  is always contained in  $\ker \mathbf{R}(\mathcal{G}, \mathbf{p})$ . Infinitesimally rigid frameworks do not admit other infinitesimal motions, which would correspond to internal deformations.

**Definition 3** (Infinitesimal rigidity). *A framework  $(\mathcal{G}, \mathbf{p})$  in  $\mathbb{R}^{nN}$  is called infinitesimally rigid if all its infinitesimal motions are Euclidean, i.e., if  $\ker \mathbf{R}(\mathcal{G}, \mathbf{p}) = \text{Eucl}_{\mathbf{p}}^n$ .*

The following result provides a basis of  $\text{Eucl}_{\mathbf{p}}^n$  and is used in Section VI. When  $n = 3$ , with  $\mathbf{e}_x, \mathbf{e}_y, \mathbf{e}_z$  the standard unit vectors in  $\mathbb{R}^3$ , define  $\mathbf{v}_{T_\xi} = \mathbf{1}_N \otimes \mathbf{e}_\xi$  as well as  $\mathbf{v}_{R_\xi} = \text{col}(\mathbf{e}_\xi \times \mathbf{p}_1, \dots, \mathbf{e}_\xi \times \mathbf{p}_N)$ , for  $\xi \in \{x, y, z\}$ . Similarly, if  $n = 2$  and  $\mathbf{e}_x, \mathbf{e}_y$  are the standard unit vectors in  $\mathbb{R}^2$ , define  $\mathbf{v}_{T_x} = \mathbf{1}_N \otimes \mathbf{e}_x$ ,  $\mathbf{v}_{T_y} = \mathbf{1}_N \otimes \mathbf{e}_y$  and

$$\mathbf{v}_{R_z} = \text{col} \left( \begin{bmatrix} -y_1 \\ x_1 \end{bmatrix}, \dots, \begin{bmatrix} -y_N \\ x_N \end{bmatrix} \right).$$

**Proposition 2.** *Suppose that  $N \geq n$ . If  $n = 2$  and at least 2 nodes are at distinct locations, the dimension of  $\text{Eucl}_{\mathbf{p}}^2$  is 3 and a basis of this subspace is given by  $(\mathbf{v}_{T_x}, \mathbf{v}_{T_y}, \mathbf{v}_{R_z})$ . If  $n = 3$  and we have at least 3 nodes that are not aligned, the dimension of  $\text{Eucl}_{\mathbf{p}}^3$  is 6 and a basis of this subspace is given by  $(\mathbf{v}_{T_x}, \mathbf{v}_{T_y}, \mathbf{v}_{T_z}, \mathbf{v}_{R_x}, \mathbf{v}_{R_y}, \mathbf{v}_{R_z})$ .*

*Proof.* We provide a proof for  $n = 3$ , the case  $n = 2$  is similar. The fact that the vectors in the proposition span  $\text{Eucl}_{\mathbf{p}}^3$  is clear by definition, so it is sufficient to prove their independence. Consider a linear combination equal to zero

$$\begin{aligned} & \alpha_1 \mathbf{v}_{T_x} + \alpha_2 \mathbf{v}_{T_y} + \alpha_3 \mathbf{v}_{T_z} + \alpha_4 \mathbf{v}_{R_x} + \alpha_5 \mathbf{v}_{R_y} + \alpha_6 \mathbf{v}_{R_z} \\ & = \text{col}(\mathbf{v} + \boldsymbol{\omega} \times \mathbf{p}_1, \dots, \mathbf{v} + \boldsymbol{\omega} \times \mathbf{p}_n) = \mathbf{0}, \end{aligned}$$

where  $\mathbf{v} = [\alpha_1, \alpha_2, \alpha_3]^T$  and  $\boldsymbol{\omega} = [\alpha_4, \alpha_5, \alpha_6]^T$ . Suppose that the nodes indexed by  $i, j$  and  $k$  are not aligned. We have from the equation above  $\mathbf{v} = -\boldsymbol{\omega} \times \mathbf{p}_i$ , and so

$$\boldsymbol{\omega} \times (\mathbf{p}_j - \mathbf{p}_i) = \boldsymbol{\omega} \times (\mathbf{p}_k - \mathbf{p}_i) = \mathbf{0}.$$

Since  $(\mathbf{p}_j - \mathbf{p}_i)$  and  $(\mathbf{p}_k - \mathbf{p}_i)$  are by assumption independent, this gives  $\boldsymbol{\omega} = \mathbf{0}$  and hence  $\mathbf{v} = \mathbf{0}$ . This proves the independence of the vectors in the proposition, which therefore form a basis of  $\text{Eucl}_{\mathbf{p}}^3$ .  $\square$

## B. Relations between the Rigidity Matrix and the FIM

Throughout this section, we consider the set of nodes (tags and anchors) to be at positions  $\mathbf{p}$ , with corresponding ranging graph  $\mathcal{G}$ . This defines a framework  $(\mathcal{G}, \mathbf{p})$ , as discussed in the previous section. The FIM  $\mathbf{F}$  is given by (5), whereas the rigidity matrix  $\mathbf{R} := \mathbf{R}(\mathcal{G}, \mathbf{p})$  is given by (13).

**Proposition 3.** *We have  $\mathbf{F} = \mathbf{R}^\top \mathbf{Q} \mathbf{R}$ , where  $\mathbf{Q} = \text{diag}(\dots, 1/(d_{ij}^{2\kappa} \sigma^2), \dots) \in \mathbb{R}^{E \times E}$ , and  $\kappa \in \{1, 2\}$  is the parameter appearing in (5).*

To explain this result, remark that  $\mathbf{F}$  in (5) has a structure similar to the Laplacian matrix  $\mathbf{L}$  of the graph  $\mathcal{G}$  [42, Chapter 12]. The expression of Proposition 3 then corresponds to the standard relationship  $\mathbf{L} = \mathbf{H}^\top \mathbf{H}$  between the incidence matrix and the usual Laplacian matrix of an undirected graph. Hence, the FIM  $\mathbf{F}$  can be considered as a weighted Laplacian matrix, noting the relation (13) between  $\mathbf{H}$  and  $\mathbf{R}$ . In [22], matrices of the form  $\mathbf{R}^\top \mathbf{Q} \mathbf{R}$ , for any diagonal matrix  $\mathbf{Q}$ , are called (weighted) ‘‘symmetric rigidity matrices’’. Hence, with this terminology, Proposition 3 says that the FIM is a symmetric rigidity matrix, for a specific set of weights in  $\mathbf{Q}$  determined by the properties of the measurement noise model. In particular, these weights depend inversely on the (true) distances between ranging nodes.

*Proof.* Starting from (13), we have

$$\mathbf{R}^\top \mathbf{Q} \mathbf{R} = (\mathbf{H}^\top \otimes \mathbf{I}_n) \text{diag} \left( \dots, \frac{\mathbf{p}_{ij} \mathbf{p}_{ij}^\top}{d_{ij}^{2\kappa} \sigma^2}, \dots \right) (\mathbf{H} \otimes \mathbf{I}_n).$$

Hence, for  $i \neq j$ , the block  $i, j$  of  $\mathbf{R}^\top \mathbf{Q} \mathbf{R}$  is

$$[\mathbf{R}^\top \mathbf{Q} \mathbf{R}]_{ij} = \sum_{e \in \mathcal{E}} H_{ei} H_{ej} \mathbf{Q}_{ee} = -\frac{\mathbf{p}_{ij} \mathbf{p}_{ij}^\top}{d_{ij}^{2\kappa} \sigma^2} \mathbf{1}_{N_i}(j) = \mathbf{F}_{ij},$$

using the fact that  $H_{ei} H_{ej} = -1$  if  $e$  is  $i \rightarrow j$  and 0 otherwise. Similarly, for all  $i$

$$[\mathbf{R}^\top \mathbf{Q} \mathbf{R}]_{ii} = \sum_{e \in \mathcal{E}} H_{ei} H_{ei} \mathbf{Q}_{ee} = \sum_{j \in N_i} \frac{\mathbf{p}_{ij} \mathbf{p}_{ij}^\top}{d_{ij}^{2\kappa} \sigma^2} = \mathbf{F}_{ii}. \quad \square$$

The following result then follows immediately from the fact that  $\mathbf{Q} \succ \mathbf{0}$  in Proposition 3.

**Corollary 1.** *We have  $\ker \mathbf{F} = \ker \mathbf{R}$ .*

The following result states that infinitesimal rigidity provides a sufficient condition for the invertibility of the symmetric positive semi-definite matrix  $\mathbf{F}_{\mathcal{U}}$  appearing in (7).

**Theorem 2.** *Suppose that the framework  $(\mathcal{G}, \mathbf{p})$  is infinitesimally rigid and contains at least  $n$  anchors at distinct locations. Moreover, when  $n = 3$ , suppose that at least 3 of these anchors are not aligned. Then  $\mathbf{F}_{\mathcal{U}}$  is invertible.*

*Proof.* We give the proof in the more involved case  $n = 3$ . With the assumed ordering of nodes and edges, the rigidity matrix has the following block structure

$$\mathbf{R} = \begin{bmatrix} \mathbf{R}_1 & \mathbf{R}_2 \\ \mathbf{0} & \mathbf{R}_3 \end{bmatrix}, \text{ with } \mathbf{R}_1 \in \mathbb{R}^{P \times U}, \mathbf{R}_3 \in \mathbb{R}^{\frac{\kappa(\kappa-1)}{2} \times K}.$$

In other words, the rows of the matrix  $\mathbf{R}_1$  correspond to the edges internal to  $\mathcal{U}$  and between  $\mathcal{U}$  and  $\mathcal{K}$ , whereas  $\mathbf{R}_3$  is the rigidity matrix of the complete subgraph formed by the anchors and the links between them. Now, we have  $\mathbf{F}_{\mathcal{U}} = \mathbf{R}_1^\top \mathbf{Q}_1 \mathbf{R}_1$ , with  $\mathbf{Q}_1$  diagonal and invertible, as in Proposition 3, so  $\ker \mathbf{F}_{\mathcal{U}} = \ker \mathbf{R}_1$ . Consider some vector  $\mathbf{x}_1 \in \mathbb{R}^U$  with  $\mathbf{x}_1 \in \ker \mathbf{R}_1$ . Then,

$$\mathbf{R} \begin{bmatrix} \mathbf{x}_1 \\ \mathbf{0} \end{bmatrix} = \begin{bmatrix} \mathbf{R}_1 & \mathbf{R}_2 \\ \mathbf{0} & \mathbf{R}_3 \end{bmatrix} \begin{bmatrix} \mathbf{x}_1 \\ \mathbf{0} \end{bmatrix} = \mathbf{0}, \quad (14)$$

hence  $\text{col}(\mathbf{x}_1, \mathbf{0})$  is in  $\ker \mathbf{R}$ . Since  $\mathcal{G}$  is infinitesimally rigid, there must exist  $\mathbf{v}, \boldsymbol{\omega}$  in  $\mathbb{R}^3$  such that

$$\begin{bmatrix} \mathbf{x}_1 \\ \mathbf{0} \end{bmatrix} = \text{col}(\mathbf{v} + \boldsymbol{\omega} \times \mathbf{p}_1, \dots, \mathbf{v} + \boldsymbol{\omega} \times \mathbf{p}_N).$$

In particular, for the 3 anchors that are not aligned, indexed by  $i, j$  and  $k$ , we must have

$$\mathbf{v} + \boldsymbol{\omega} \times \mathbf{p}_i = \mathbf{v} + \boldsymbol{\omega} \times \mathbf{p}_j = \mathbf{v} + \boldsymbol{\omega} \times \mathbf{p}_k = \mathbf{0}.$$

From this, we conclude as in the proof of Proposition 2 that  $\mathbf{v} = \boldsymbol{\omega} = \mathbf{0}$ , which in turns implies  $\mathbf{x}_1 = \mathbf{0}$ . Hence  $\ker \mathbf{F}_{\mathcal{U}} = \{\mathbf{0}\}$ , i.e.,  $\mathbf{F}_{\mathcal{U}} \succ \mathbf{0}$ .  $\square$

**Remark 5.** *If we have only one tag, then one can show that  $\mathbf{F}_{\mathcal{U}}$  is invertible if and only if we have at least  $n$  anchors and the nodes' locations span an affine space of full dimension  $n$  (i.e., we have 3 non aligned nodes if  $n = 2$ , and 4 non coplanar nodes if  $n = 3$ ). Note that if we have only  $n$  anchors, we cannot localize uniquely the tag in general, even with perfect measurements, because the intersection of  $n$  spheres in  $\mathbb{R}^n$  gives two possible locations. Hence, even when  $\mathbf{F}_{\mathcal{U}}$  is invertible, the localization problem might not be uniquely solvable. Unicity of the localization solution can be characterized by the stronger notion of global rigidity [14], which however is more complex to check if  $n = 2$  and for which no exact test is currently known if  $n = 3$ .*

Theorem 2 can be used to produce an initial node placement and choose ranging links to guarantee that  $\mathbf{F}_{\mathcal{U}}$  is already invertible at the start of the deployment. For this, we should ensure that  $(\mathcal{G}, \mathbf{p})$  is infinitesimally rigid. One convenient way to satisfy this condition (in fact, the stronger condition of global rigidity) is to construct a *triangulation graph* [14], [43]: starting from a set of at least  $n + 1$  anchors, we add tags one by one, with each new tag connected to at least  $n + 1$  previous nodes that are in general position (3 non-aligned nodes if  $n = 2$ , 4 non-coplanar nodes if  $n = 3$ ). Although this construction requires more anchors and links than the strict minimum necessary for the invertibility of  $\mathbf{F}_{\mathcal{U}}$ , the resulting network supports efficient distributed localization algorithms that are robust to measurement noise [43].

## V. DISTRIBUTED GRADIENT COMPUTATIONS FOR THE LOCALIZABILITY POTENTIALS

In order to implement the gradient descent scheme (3), in Section V-A we provide analytical forms for the gradients of the localizability potentials (9), (10) and (11). Then, in Sections V-B and V-C, we describe decentralized deployment

algorithms by showing how each agent can compute its components of the gradient of the chosen localizability potential, using its own local information as well as data obtained from its neighbors in the ranging graph.

### A. Partial Derivatives of the FIM

Irrespective to the potential considered, we need to evaluate the derivative of the FIM  $\mathbf{F}_{\mathcal{U}}$  in (7) with respect to any coordinate  $\xi_i \in \{x_i, y_i, z_i\}$  of a mobile agent  $i$  (anchor or tag) located at  $\mathbf{p}_i = [x_i, y_i, z_i]^\top$ . We provide formulas for the case  $n = 3$ , the case  $n = 2$  being similar. Define the notation  $\xi_{ij} = \xi_i - \xi_j$  and  $\gamma_{ij} = \frac{\kappa}{\sigma^2 d_{ij}^{2(\kappa+1)}} \mathbf{1}_{\mathcal{N}_i}(j)$ . For  $\mathbf{F}_{ij}$ ,  $i \neq j$ , the  $3 \times 3$  blocks introduced in (5), we find

$$\begin{aligned} \frac{\partial \mathbf{F}_{ij}}{\partial x_i} &= \gamma_{ij} \begin{bmatrix} x_{ij}^3 - \frac{d_{ij}^2 x_{ij}}{\kappa} & x_{ij}^2 y_{ij} - \frac{d_{ij}^2 y_{ij}}{2\kappa} & x_{ij}^2 z_{ij} - \frac{d_{ij}^2 z_{ij}}{2\kappa} \\ \star & x_{ij} y_{ij}^2 & x_{ij} y_{ij} z_{ij} \\ \star & \star & x_{ij} z_{ij}^2 \end{bmatrix} \\ \frac{\partial \mathbf{F}_{ij}}{\partial y_i} &= \gamma_{ij} \begin{bmatrix} x_{ij}^2 y_{ij} & x_{ij} y_{ij}^2 - \frac{d_{ij}^2 x_{ij}}{2\kappa} & x_{ij} y_{ij} z_{ij} \\ \star & y_{ij}^3 - \frac{d_{ij}^2 y_{ij}}{\kappa} & y_{ij}^2 z_{ij} - \frac{d_{ij}^2 z_{ij}}{2\kappa} \\ \star & \star & y_{ij} z_{ij}^2 \end{bmatrix}, \\ \frac{\partial \mathbf{F}_{ij}}{\partial z_i} &= \gamma_{ij} \begin{bmatrix} x_{ij}^2 z_{ij} & x_{ij} y_{ij} z_{ij} & x_{ij} z_{ij}^2 - \frac{d_{ij}^2 x_{ij}}{2\kappa} \\ \star & y_{ij}^2 z_{ij} & y_{ij} z_{ij}^2 - \frac{d_{ij}^2 y_{ij}}{2\kappa} \\ \star & \star & z_{ij}^3 - \frac{d_{ij}^2 z_{ij}}{\kappa} \end{bmatrix}, \quad (15) \end{aligned}$$

where the symbol  $\star$  replaces symmetric terms. These expressions are sufficient to compute the whole matrix  $\partial \mathbf{F}_{\mathcal{U}} / \partial \xi_i$ , because  $\mathbf{F}_{ji} = \mathbf{F}_{ij}$ ,  $\mathbf{F}_{aa} = -\sum_{b \in \mathcal{N}_a} \mathbf{F}_{ab}$ , and  $\partial \mathbf{F}_{ab} / \partial \xi_i = \mathbf{0}$  if  $a \neq b$  and  $i \notin \{a, b\}$ .

Using standard differentiation rules [40], the partial derivatives of the A-Opt potential (9) are

$$\frac{\partial J_A(\mathbf{p})}{\partial \xi_i} = \frac{\partial \text{Tr} \{ \mathbf{F}_{\mathcal{U}}^{-1} \}}{\partial \xi_i} = -\text{Tr} \left\{ \mathbf{F}_{\mathcal{U}}^{-2} \frac{\partial \mathbf{F}_{\mathcal{U}}}{\partial \xi_i} \right\}. \quad (16)$$

Similarly, we can compute the derivatives of the D-Opt potential (10) as

$$\frac{\partial J_D(\mathbf{p})}{\partial \xi_i} = -\frac{\partial \ln \det \mathbf{F}_{\mathcal{U}}}{\partial \xi_i} = -\text{Tr} \left\{ \mathbf{F}_{\mathcal{U}}^{-1} \frac{\partial \mathbf{F}_{\mathcal{U}}}{\partial \xi_i} \right\}. \quad (17)$$

Finally, if  $\lambda_{\min}(\mathbf{F}_{\mathcal{U}})$  is a non-repeated eigenvalue with associated unit norm eigenvector  $\mathbf{v}$ , we can compute the derivative of the E-Opt potential (11) as [44, p. 565]

$$\frac{\partial J_E(\mathbf{p})}{\partial \xi_i} = -\frac{\partial \lambda_{\min}(\mathbf{p})}{\partial \xi_i} = -\mathbf{v}^\top \frac{\partial \mathbf{F}_{\mathcal{U}}}{\partial \xi_i} \mathbf{v}. \quad (18)$$

Hence, we can in principle compute the gradient of the chosen localizability potential, using the expressions for the FIM and its derivatives. However, in practice we would also like to be able to implement these computations in a distributed manner, in order to obtain deployment strategies that can be used by an MRS with incomplete ranging graph  $\mathcal{G}$ , assuming communication over this ranging graph is also possible.

### B. Decentralized Gradient Computations for the D- and A-Opt Potentials

We propose now a new method to estimate in a distributed way the gradient of the D- and A-Opt potentials at a given configuration  $\mathbf{p}$ , which have similar expressions, see (16) and (17). As mentioned in Remark 1, we assume that each node  $i$  has access to its position  $\mathbf{p}_i$ , which could be its true position (e.g., for anchors) or an estimate obtained after executing a localization algorithm such as the one in [43]. In the latter case, the algorithms presented here will simply produce the gradient of  $J_{\text{loc}}$  at the estimated position. In the following, we omit  $\mathbf{p}$  from the notation, writing  $\mathbf{F}_{\mathcal{U}}$  instead of  $\mathbf{F}_{\mathcal{U}}(\mathbf{p})$ . The method essentially relies on inverting  $\mathbf{F}_{\mathcal{U}}$  in a decentralized manner, which we discuss first.

1) *Auxiliary Problem:* Suppose that each tag  $i \in \mathcal{U}$  knows initially a matrix  $\mathbf{E}_i \in \mathbb{R}^{n \times m}$ , for some integer  $m$ , and the tags need to compute  $\mathbf{F}_{\mathcal{U}}^{-1}\mathbf{E}$  in a distributed manner over the network  $\mathcal{G}$ , where  $\mathbf{E} = \text{col}(\mathbf{E}_1, \dots, \mathbf{E}_U) \in \mathbb{R}^{nU \times m}$ . This is equivalent to solving in a decentralized manner the linear system  $\mathbf{F}_{\mathcal{U}}\mathbf{X} = \mathbf{E}$ , with the matrix variable  $\mathbf{X} \in \mathbb{R}^{nU \times m}$ . A special case of this problem is to compute  $\mathbf{F}_{\mathcal{U}}^{-1}$ , when  $\mathbf{E} = \mathbf{I}_{nU}$ .

Consider the following system of differential equations

$$\dot{\mathbf{X}}(t) = -\mathbf{F}_{\mathcal{U}}\mathbf{X}(t) + \mathbf{E}, \quad \mathbf{X}(0) = \mathbf{X}_0. \quad (19)$$

If  $\mathbf{F}_{\mathcal{U}} \succ \mathbf{0}$ , as guaranteed by Theorem 2, then  $-\mathbf{F}_{\mathcal{U}}$  has strictly negative eigenvalues, i.e., is stable, so the solution  $\mathbf{X}(t)$  to the system (19) converges to the solution  $\mathbf{F}_{\mathcal{U}}^{-1}\mathbf{E}$  of the linear system as  $t \rightarrow \infty$ , no matter the choice of initial condition  $\mathbf{X}_0$ . A discrete-time version of the flow (19) can be implemented for  $l \geq 0$  as

$$\mathbf{X}_{l+1} = \mathbf{X}_l - \eta_l (\mathbf{F}_{\mathcal{U}}\mathbf{X}_l - \mathbf{E}),$$

for some stepsizes  $\eta_l$ , which reads more explicitly for each tag  $1 \leq i \leq U$

$$\begin{aligned} \mathbf{X}_{i,l+1} = & \eta_l \sum_{j \in \mathcal{N}_i \cap \mathcal{U}} \mathbf{F}_{ij}(\mathbf{X}_{i,l} - \mathbf{X}_{j,l}) \\ & + \left( \mathbf{I}_n + \eta_l \sum_{j \in \mathcal{N}_i \cap \mathcal{K}} \mathbf{F}_{ij} \right) \mathbf{X}_{i,l} + \eta_l \mathbf{E}_i. \end{aligned} \quad (20)$$

Again, the iterates  $\mathbf{X}_k$  converge to the desired solution  $\mathbf{F}_{\mathcal{U}}^{-1}\mathbf{E}$  if we choose for example  $\eta_l = \eta$  constant and sufficiently small (namely, as long as  $\eta < 2/\lambda_{\max}(\mathbf{F}_{\mathcal{U}})$ ). The iterations (20) can be implemented in a decentralized manner by the tags, i.e., at each step  $l$  tag  $i$  only needs to exchange its matrix  $\mathbf{X}_i$  with its neighboring tags. This also requires that tag  $i$  knows  $\mathbf{F}_{ij}$  for  $j \in \mathcal{N}_i$ , which is the case if prior to the iterations, the nodes (tags and anchors) broadcast their position (estimates) to their neighbors. When the iterations have converged, the  $n \times m$  matrix  $\mathbf{X}_i$  at tag  $i$  represents the  $i^{\text{th}}$  block of rows of  $\mathbf{F}_{\mathcal{U}}^{-1}\mathbf{E}$ , i.e.,  $\mathbf{F}_{\mathcal{U}}^{-1}\mathbf{E} = \text{col}(\mathbf{X}_1, \dots, \mathbf{X}_U)$ .

**Remark 6.** The iterations (20) correspond to Richardson iterations to solve the linear system  $\mathbf{F}_{\mathcal{U}}\mathbf{X} = \mathbf{E}$  in a decentralized

way [45]. Other distributed iterative methods could be used, such as the Jacobi over-relaxation iterations

$$\mathbf{X}_{i,l+1} = (1 - \eta) \mathbf{X}_{i,l} + \eta \mathbf{F}_{ii}^{-1} \left( \mathbf{E}_i - \sum_{j \in \mathcal{N}_i \cap \mathcal{U}} \mathbf{F}_{ij} \mathbf{X}_{j,l} \right),$$

with potentially better convergence properties, but a detailed discussion of such alternatives, which can be found in [45, Chapter 2], is outside of the scope of this paper.

2) *Application to compute  $\partial J_D / \partial \xi_i$ :* To implement the gradient descent scheme (3) for D-optimization, each mobile node  $i$  (tag or anchor) needs to compute  $\partial J_D / \partial \xi_i$  for  $\xi_i \in \{x_i, y_i, z_i\}$ , which is given by (17). Denote  $\mathbf{M} = \mathbf{F}_{\mathcal{U}}^{-1} \in \mathbb{R}^{nU \times nU}$  and its  $n \times n$  blocks  $\mathbf{M}_{ij}$ , for  $1 \leq i, j \leq U$ . First, the tags run the iterations (20), with the matrix  $\mathbf{E} = \mathbf{I}_{nU}$ . That is, tag  $j$  uses the matrix  $\mathbf{E}_j = \mathbf{e}_j^{\top} \otimes \mathbf{I}_n$ , where  $\mathbf{e}_j$  is the  $j^{\text{th}}$  unit vector in  $\mathbb{R}^U$ . After convergence, tag  $j$  stores an approximation of the matrix  $\mathbf{M}_j = [\mathbf{M}_{j1}, \dots, \mathbf{M}_{jU}] \in \mathbb{R}^{n \times nU}$ . A stopping condition  $\max_{i \in \mathcal{N}_j} \|\mathbf{X}_{i,l+1} - \mathbf{X}_{i,l}\| / \|\mathbf{X}_{i,l}\| < \epsilon$  can be implemented at each node  $j$ , for a threshold  $\epsilon > 0$ .

Next, note from (15) that the only  $n \times n$  non-zero blocks  $\partial \mathbf{F}_{ab} / \partial \xi_i$ , with  $0 \leq a, b \leq U$ , are those for which: i)  $a = b$  and  $a \in \mathcal{N}_i$ ; ii)  $a = b = i$ ; iii)  $a = i$  and  $b \in \mathcal{N}_i$ ; or iv)  $b = i$  and  $a \in \mathcal{N}_i$ . Moreover, if  $i$  is a mobile anchor (so  $i \geq U + 1$ ), only case i) can occur. From this remark, we can derive the following expressions. If  $i \in \mathcal{U}$

$$\begin{aligned} \frac{\partial J_D(\mathbf{p})}{\partial \xi_i} = & \sum_{j \in \mathcal{N}_i \cap \mathcal{U}} \text{Tr} \left\{ (\mathbf{M}_{jj} + \mathbf{M}_{ii} - 2\mathbf{M}_{ij}) \frac{\partial \mathbf{F}_{ij}}{\partial \xi_i} \right\} \\ & + \sum_{j \in \mathcal{N}_i \cap \mathcal{K}} \text{Tr} \left\{ \mathbf{M}_{ii} \frac{\partial \mathbf{F}_{ij}}{\partial \xi_i} \right\}, \end{aligned} \quad (21)$$

and if  $i \in \mathcal{K}$

$$\frac{\partial J_D(\mathbf{p})}{\partial \xi_i} = \sum_{j \in \mathcal{N}_i \cap \mathcal{U}} \text{Tr} \left\{ \mathbf{M}_{jj} \frac{\partial \mathbf{F}_{ij}}{\partial \xi_i} \right\}. \quad (22)$$

Assuming that each node knows an estimate of its coordinates and of its neighbors' coordinates, node  $i$  can obtain from its neighbor tags  $j$  the terms  $\text{Tr} \{ \mathbf{M}_{jj} \partial \mathbf{F}_{ij} / \partial \xi_i \}$ , and also compute the terms  $\text{Tr} \{ \mathbf{M}_{ii} \partial \mathbf{F}_{ij} / \partial \xi_i \}$  and  $\text{Tr} \{ \mathbf{M}_{ij} \partial \mathbf{F}_{ij} / \partial \xi_i \}$  if  $i \in \mathcal{U}$ . Hence, overall this provides a method allowing each mobile node  $i$  to compute  $\partial J_D / \partial \xi_i$  by communicating only with its neighbors. Nevertheless, it requires significant data exchanges between the agents (exchanges to reach the convergence in (20) and sending of the approximations of  $\mathbf{M}_j$ , of size  $n \times nU$ , to the neighbors), which can limit its scalability to large MRS. Algorithm 1 summarizes the distributed gradient computation procedure for D-optimization.

The same steps can be used to compute the gradient (16) at each mobile node for A-optimization. The only difference is that the matrices  $\mathbf{M}_i$  above should represent rows of  $\mathbf{F}_{\mathcal{U}}^{-2}$  instead of  $\mathbf{F}_{\mathcal{U}}^{-1}$ . For this, the tags first compute the rows  $\bar{\mathbf{M}}_i$  of  $\mathbf{F}_{\mathcal{U}}^{-1}$  using the iterations (20). Then, we restart these iterations but now replacing the matrices  $\mathbf{E}_i = \mathbf{e}_i^{\top} \otimes \mathbf{I}_n$  by  $\bar{\mathbf{M}}_i$ . This computes an approximation of  $\mathbf{F}_{\mathcal{U}}^{-1} \mathbf{F}_{\mathcal{U}}^{-1} = \mathbf{F}_{\mathcal{U}}^{-2}$ , as desired. However, the resulting distributed A-Opt scheme requires more computational resources and communication exchanges and is thus less applicable for large MRS.



**Algorithm 1:** D-Opt distributed gradient computation

**Data:** Each node  $i$  knows an estimate of its  $\mathbf{p}_i$  from a localization algorithm, or exactly if  $i \in \mathcal{K}$   
**Result:** Each mobile node  $i$  knows  $\partial J_D(\mathbf{p})/\partial \mathbf{p}_i$   
Each node  $i \in \mathcal{U} \cup \mathcal{K}$  broadcasts  $\mathbf{p}_i$  to its neighbors;  
The tags run the iterations (20) until convergence, with  $\mathbf{E}_j = \mathbf{e}_j^\top \otimes \mathbf{I}_n$  for tag  $j$ , and each tag  $j$  stores the resulting matrix  $\mathbf{M}_j$ ;  
Each mobile tag  $i$  computes  $\sum_{j \in \mathcal{N}_i} \text{Tr} \left\{ (\mathbf{M}_{ii} - 2\mathbf{M}_{ij} \mathbf{1}_{\mathcal{K}}(j)) \frac{\partial \mathbf{F}_{ij}}{\partial \xi_i} \right\}$ ;  
Each tag  $j$  computes and sends  $\text{Tr} \left\{ \mathbf{M}_{jj} \frac{\partial \mathbf{F}_{ij}}{\partial \xi_i} \right\}$  to each of its mobile neighbors  $i \in \mathcal{N}_j$  ( $i$  tag or anchor);  
Each mobile node  $i$  computes its gradient using (21) or (22);

**C. Decentralized Computation of E-Opt Gradient**

The decentralized computation of the gradient of the E-Opt potential can be done using the methodology developed in [19] for the standard Laplacian, also used in [22] for the symmetric rigidity matrix. Hence, our presentation is brief and focuses on adapting this methodology to  $\mathbf{F}_{\mathcal{U}}(\mathbf{p})$ .

Using the sparsity of  $\mathbf{F}_{\mathcal{U}}$ , if  $i \in \mathcal{U}$ , we can rewrite (18) as

$$\begin{aligned} \frac{\partial J_E(\mathbf{p})}{\partial \xi_i} &= \sum_{j \in \mathcal{N}_i \cap \mathcal{U}} (\mathbf{v}_i - \mathbf{v}_j)^T \frac{\partial \mathbf{F}_{ij}}{\partial \xi_i} (\mathbf{v}_i - \mathbf{v}_j)^T \\ &+ \mathbf{v}_i^T \left( \sum_{j \in \mathcal{N}_i \cap \mathcal{K}} \frac{\partial \mathbf{F}_{ij}}{\partial \xi_i} \right) \mathbf{v}_i, \end{aligned} \quad (23)$$

and if  $i \in \mathcal{K}$

$$\frac{\partial J_E(\mathbf{p})}{\partial \xi_i} = \sum_{j \in \mathcal{N}_i \cap \mathcal{U}} \mathbf{v}_j^\top \frac{\partial \mathbf{F}_{ij}}{\partial \xi_i} \mathbf{v}_j, \quad (24)$$

where  $\mathbf{v} = \text{col}(\mathbf{v}_1, \dots, \mathbf{v}_U) \in \mathbb{R}^{nU}$ . Computing these expressions requires a decentralized algorithm to estimate the components of  $\mathbf{v}$ , a unit norm eigenvector associated with  $\lambda_1 := \lambda_{\min}(\mathbf{F}_{\mathcal{U}})$ .

1) *Power-iteration eigenvector estimator:* To compute  $\mathbf{v}$  in a decentralized manner, consider the solution  $t \mapsto \mathbf{w}(t) \in \mathbb{R}^{nU}$  to the following differential equation, adapted from [19],

$$\dot{\mathbf{w}} = -[\beta \mathbf{F}_{\mathcal{U}} + \mu((nU)^{-1} \|\mathbf{w}(t)\|^2 - 1) \mathbf{I}_{nU}] \mathbf{w}(t), \quad (25)$$

with an initial condition  $\mathbf{w}_0 := \mathbf{w}(0)$  and  $\beta, \mu > 0$ .

**Proposition 4.** *If  $\mu > \lambda_1 \beta$  and  $\mathbf{w}_0^\top \mathbf{v} \neq 0$ , then the solution  $\mathbf{w}(t)$  to (25) converges to an eigenvector  $\mathbf{w}_\infty$  of  $\mathbf{F}_{\mathcal{U}}$ , associated with  $\lambda_1$  and proportional to  $\mathbf{v}$ .*

*Proof.* This follows from the argument in the appendix of [19].  $\square$

In practice, we can choose  $\mathbf{w}_0$  randomly to fulfill the condition  $\mathbf{w}_0^\top \mathbf{v} \neq 0$  with probability one. To set the gains  $\beta, \mu$ , note that  $\text{Tr} \{\mathbf{F}_{\mathcal{U}}\} > \lambda_1$  since  $\mathbf{F}_{\mathcal{U}} \succ 0$ . Then, for the additive measurement noise model (1), we have  $\text{Tr} \{\mathbf{F}_{\mathcal{U}}\} \leq \frac{2P}{\sigma^2}$ . So, if we choose  $\beta \geq \sigma^2/(2P)$  and  $\mu > 1$ , the condition of Proposition 4 is satisfied. For the log-normal model (2), we

have  $\text{Tr} \{\mathbf{F}_{\mathcal{U}}\} \leq \frac{2}{\sigma^2} \sum_{\{i,j\} \in \mathcal{E}, i \in \mathcal{U}} d_{ij}^{-2}$ . Hence, if we set again  $\beta \geq \sigma^2/(2P)$  and now  $\mu > 1/d_{\min}^2$ , such that  $d_{ij} \geq d_{\min}$  for all  $i, j$ , then the condition of Proposition 4 is satisfied. The minimum distance  $d_{\min}$  between robots could be enforced as part of a collision avoidance scheme.

An estimation algorithm for  $\mathbf{v}$  is obtained by discretizing (25), leading to the following iterations for each agent  $i \in \mathcal{U}$

$$\begin{aligned} \mathbf{w}_{i,l+1} &= \mathbf{w}_{i,l} - \eta_l \left( \mu(s_l - 1) \mathbf{w}_{i,l} \right. \\ &\quad \left. + \beta \sum_{a \in (\mathcal{N}_i \cup \{i\}) \cap \mathcal{U}} \mathbf{F}_{il} \mathbf{w}_{a,l} \right), \end{aligned} \quad (26)$$

where  $\eta_l > 0$  is a sufficiently small step-size and  $s_l := \|\mathbf{w}_l\|^2/nU$ . All the terms in (26) can be obtained locally by node  $i$  using one-hop communication with its neighbors, except for the global average  $s_l$ , which can be computed by a consensus algorithm as described next. The last step is to normalize  $\mathbf{w}_\infty$ , obtained after convergence in (26). This can again be done by each individual agent, since  $\mathbf{v} := \mathbf{w}_\infty/\sqrt{nUs_\infty}$  is a unit-norm vector.

2) *Estimation of  $s_l$  via a consensus algorithm:* Since  $s_l = \|\mathbf{w}_l\|^2/(nU) = \frac{1}{U} \sum_{i=1}^U (\|\mathbf{w}_{i,l}\|^2/n)$ , this term can be computed by the tags using a decentralized averaging consensus algorithm. We assume for simplicity that the graph of the tags  $\mathcal{G}_{\mathcal{U}}$  is connected. To solve the averaging problem, each tag  $i$  initializes a variable  $\hat{s}_{i,l,0} := \|\mathbf{w}_{i,l}\|^2/n$ . Then, they execute in a distributed manner the iterations

$$\hat{s}_{l,m+1} = \mathbf{G} \hat{s}_{l,m}, \quad \forall m \geq 0, \quad (27)$$

where  $\hat{s}_{l,m} = \text{col}(\hat{s}_{1,l,m}, \dots, \hat{s}_{U,l,m})$ , and  $\mathbf{G}$  is a doubly stochastic matrix of weights  $G_{ij}$  associated with the edges of  $\mathcal{G}_{\mathcal{U}}$  (i.e.,  $\sum_{u=1}^U G_{iu} = \sum_{u=1}^U G_{ui} = 1$ , for  $1 \leq i \leq U$ , and  $G_{ij} = 0$  if  $j \notin \mathcal{N}_i$ ), for instance the Metropolis-Hastings weights

$$\begin{cases} G_{ij} = \mathbf{1}_{\mathcal{N}_i \cap \mathcal{U}}(j) (1 + \max(|\mathcal{N}_i|, |\mathcal{N}_j|))^{-1}, \forall i \neq j, \\ G_{ii} = 1 - \sum_{u=1}^U G_{iu}. \end{cases}$$

We then have  $\hat{s}_{l,m} \rightarrow s_l \mathbf{1}_U$  [37, p. 58], so that each tag knows after convergence the scalar value  $s_l$  needed for (26).

**Remark 7.** *Since  $s_l$  is time varying and we need to track its value at each period  $l$ , dynamic consensus methods [46] may converge faster than the solution presented here. We leave the exploration of such schemes for future work.*

Algorithm 2 summarizes the decentralized computation of the estimate  $\hat{\mathbf{v}}_i$  of the  $i$ -th component of  $\mathbf{v}$  by a given tag  $i \in \mathcal{U}$ . After decentralized estimation of  $\mathbf{v}$  by the tags, each mobile agent  $i$  can compute its components of the gradient of  $J_E$  from (23) or (24) by communicating with its neighbors.

**Remark 8.** *When the subgraph of  $\mathcal{G}$  with only the tags is not connected, it is still possible to distributively compute the gradient of  $J_E$ . In this case, there exists a  $U \times U$  permutation matrix  $\mathbf{P}$  such that  $\hat{\mathbf{F}}_{\mathcal{U}} = (\mathbf{P} \otimes \mathbf{I}_n)^{-1} \mathbf{F}_{\mathcal{U}} (\mathbf{P} \otimes \mathbf{I}_n) = \text{diag}(\mathbf{F}_{S_1} \dots \mathbf{F}_{S_L} \dots)$  is block diagonal, where each  $S_l$  represents a subset of connected tags. Hence, the minimal eigenvalue  $\lambda$  of  $\mathbf{F}_{\mathcal{U}}$  is among the minimal eigenvalues  $\lambda_{S_l}$  of the blocks  $\mathbf{F}_{S_l}$ . Therefore, each subset  $S_l$  can use*

**Algorithm 2:** Estimation of  $\mathbf{v}_i$  by tag  $i \in \mathcal{U}$ .

---

**Data:**  $\mathbf{w}_{i,0}$  random,  $\mathbf{G}$ ,  $\mu$ ,  $\beta$ ,  $n_{\text{iter}}$ ,  $\tilde{n}_{\text{iter}}$

**for**  $0 \leq l \leq n_{\text{iter}}$  **do**

$\hat{\mathbf{s}}_{i,l,0} = \|\mathbf{w}_{i,l}\|^2/n$ ;

**for**  $0 \leq m \leq \tilde{n}_{\text{iter}}$  **do**

$\hat{\mathbf{s}}_{i,l,m+1} = \mathbf{G}_{ii}\hat{\mathbf{s}}_{i,l,m} + \sum_{j \in \mathcal{N}_i \cap \mathcal{U}} \mathbf{G}_{ij}\hat{\mathbf{s}}_{j,l,m}$ ;

**end**

**compute**  $\mathbf{w}_{i,l+1}$ , setting  $s_l := \hat{\mathbf{s}}_{i,\tilde{n}_{\text{iter}}}$  in (26).

**end**

**transmit**  $\hat{\mathbf{v}}_i := \frac{\mathbf{w}_{i,n_{\text{iter}}}}{\sqrt{nU\hat{\mathbf{s}}_{i,n_{\text{iter}}}}}$  to the neighborhood;

---

Algorithm 2 to compute its eigenvector  $\mathbf{v}_{S_i}$  associated to  $\lambda_{S_i} := \mathbf{v}_{S_i}^\top \mathbf{F}_{S_i} \mathbf{v}_{S_i}$ . On the other hand, the graph  $\mathcal{G}$  with all nodes is assumed rigid and hence fully connected. This allows comparing the  $\lambda_{S_i}$  through the network  $\mathcal{K}$  formed by the anchors in order to find  $\lambda := \min_{S_i} \lambda_{S_i}$  corresponding to the subset  $\mathcal{S}^*$ . Since  $\mathbf{F}_{\mathcal{U}}$  is block diagonal, its eigenvector associated with  $\lambda$  is  $\text{col}(0, \dots, \mathbf{v}_{S^*}, \dots, 0)$ , which then yields  $\mathbf{v} = (\mathbf{P} \otimes \mathbf{I}_n) \text{col}(0, \dots, \mathbf{v}_{S^*}, \dots, 0)$  for  $\mathbf{F}_{\mathcal{U}}$ . Then,  $\mathbf{v}$  gives the gradient of  $J_E$  using (23) and (24).

## VI. LOCALIZABILITY OPTIMIZATION FOR RIGID BODIES

## A. Constrained Localizability Optimization

In this section, we consider scenarios where mobile robots can carry several tags, see Fig. 2. Hence, the relative motion and position of some tags are constrained by the fact that they are attached to the same rigid body. More generally, let  $\mathbf{f}_c : \mathbf{R}^{nU} \rightarrow \mathbf{R}^C$  be a known function defining  $C$  constraints  $\mathbf{f}_c(\mathbf{p}_{\mathcal{U}}) = \mathbf{0}$  that the tag positions must satisfy, and define the feasible set

$$\mathcal{C} := \{\mathbf{p} = \text{col}(\mathbf{p}_{\mathcal{U}}, \mathbf{p}_{\mathcal{K}}) \in \mathbb{R}^{nN} \mid \mathbf{f}_c(\mathbf{p}_{\mathcal{U}}) = \mathbf{0}\}. \quad (28)$$

To use the CRLB as localizability potential, the bound should now reflect the fact that localization algorithms can leverage the information provided by the constraints to improve their performance. We use the following result generalizing Proposition 1.

**Proposition 5.** Assume that the tag positions are subject to the constraints (28). Let  $\mathbf{A}_{\mathcal{U}}(\mathbf{p}_{\mathcal{U}})$  be a matrix whose columns span  $\ker \partial \mathbf{f}_c / \partial \mathbf{p}_{\mathcal{U}}$  (which depends on  $\mathbf{p}_{\mathcal{U}}$  in general). Let  $\hat{\mathbf{p}}_{\mathcal{U}}$  be an unbiased estimate of the tag positions  $\mathbf{p}_{\mathcal{U}}$ , based on the measurements  $\tilde{\mathbf{d}}$ , the knowledge of the anchor positions  $\mathbf{p}_{\mathcal{K}}$ , and the knowledge of the constraints (28). Then

$$\text{cov}[\hat{\mathbf{p}}_{\mathcal{U}}] \succeq \mathbf{B}_{\mathcal{U}}(\mathbf{p}), \quad (29)$$

where

$$\mathbf{B}_{\mathcal{U}}(\mathbf{p}) := \mathbf{A}_{\mathcal{U}}[\mathbf{A}_{\mathcal{U}}^T \mathbf{F}_{\mathcal{U}} \mathbf{A}_{\mathcal{U}}]^\dagger \mathbf{A}_{\mathcal{U}}^T. \quad (30)$$

*Proof.* We have both the trivial constraint  $\mathbf{f}_t(\mathbf{p}_{\mathcal{U}}) = \mathbf{p}_{\mathcal{K}} - \mathbf{p}_{\mathcal{K}}^* = \mathbf{0}$  with  $\mathbf{p}_{\mathcal{K}}^*$  the known positions of the anchors, and the equality constraint  $\mathbf{f}_c(\mathbf{p}_{\mathcal{U}}) = \mathbf{0}$ . Define  $\mathbf{h}(\mathbf{p}) = \text{col}(\mathbf{f}_c(\mathbf{p}_{\mathcal{U}}), \mathbf{f}_t(\mathbf{p}_{\mathcal{K}}))$ . We then have :

$$\frac{\partial \mathbf{h}}{\partial \mathbf{p}} = \begin{bmatrix} \frac{\partial \mathbf{f}_c}{\partial \mathbf{p}_{\mathcal{U}}} & \mathbf{0} \\ \mathbf{0} & \mathbf{I}_{nK} \end{bmatrix}.$$

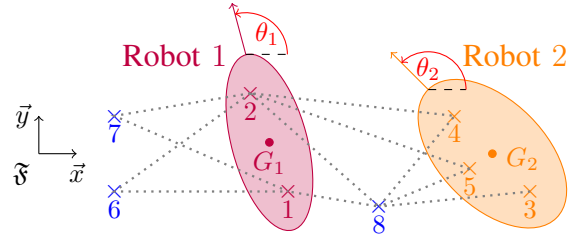


Fig. 2: Setup for two robots, seen as rigid bodies, carrying multiple tags.

We apply the result of Theorem 1, with the matrix  $\mathbf{A}$  in (6)

$$\mathbf{A} = \begin{bmatrix} \mathbf{A}_{\mathcal{U}} \\ \mathbf{0} \end{bmatrix} \text{ so } \mathbf{F}_c = \mathbf{A}_{\mathcal{U}}^\top \mathbf{F}_{\mathcal{U}} \mathbf{A}_{\mathcal{U}}, \quad \mathbf{B}_c = \begin{bmatrix} \mathbf{A}_{\mathcal{U}} \mathbf{F}_c^\dagger \mathbf{A}_{\mathcal{U}}^\top & \mathbf{0} \\ \mathbf{0} & \mathbf{0} \end{bmatrix}.$$

In (6), the  $nU \times nU$  top-left corner of the matrix inequality gives (29) for the covariance of  $\hat{\mathbf{p}}_{\mathcal{U}}$ . The other parts of the bound (6) are trivial ( $\mathbf{0} \succeq \mathbf{0}$ ) and correspond to the fact that a reasonable estimate  $\hat{\mathbf{p}} = \text{col}(\hat{\mathbf{p}}_{\mathcal{U}}, \hat{\mathbf{p}}_{\mathcal{K}})$  should set  $\hat{\mathbf{p}}_{\mathcal{K}} = \mathbf{p}_{\mathcal{K}}$ , so that  $\hat{\mathbf{p}}_{\mathcal{K}}$  will have zero covariance.  $\square$

Note that to simplify the notation, we have omitted in (30) to state the dependencies  $\mathbf{A}_{\mathcal{U}}(\mathbf{p}_{\mathcal{U}})$  and  $\mathbf{F}_{\mathcal{U}}(\mathbf{p})$ . From the matrix-valued bound (30), we can define constrained localizability potentials as in Section III-B. Here, for conciseness, we only consider the A-Opt potential

$$J_c(\mathbf{p}) := \text{Tr} \{\mathbf{B}_{\mathcal{U}}(\mathbf{p})\}. \quad (31)$$

Moreover, the desired tag positions should also respect the constraints specified by (28). In other words, we aim to adjust the positions of the mobile nodes (anchors or tags) in order to minimize, at least locally, the overall potential  $J$ , which includes the localizability potential  $J_c$  in (31), subject to the constraints (28). For this, we can replace the gradient-descent method (3) by the following first-order primal-dual method [47, p. 528]:

$$\begin{cases} \mathbf{p}_{k+1} = \mathbf{p}_k - \eta_k \left( \frac{\partial J(\mathbf{p}_k)}{\partial \mathbf{p}} + \boldsymbol{\lambda}_k^T \frac{\partial \mathbf{f}_c(\mathbf{p}_{\mathcal{U},k})}{\partial \mathbf{p}} \right)^T, \\ \boldsymbol{\lambda}_{k+1} = \boldsymbol{\lambda}_k + \delta \mathbf{f}_c(\mathbf{p}_{\mathcal{U},k}), \end{cases} \quad (32)$$

where  $\eta_k \in \mathbb{R}$  is a sequence of stepsizes,  $\delta$  a fixed parameter and  $\boldsymbol{\lambda}_k$  are dual variable iterates. The scheme (32) provides a sequence of configurations  $\mathbf{p}_k$ ,  $k \geq 0$ . Feasibility of the constraints (28) is not maintained during the iterations (32), but the algorithm contributes to keeping  $\mathbf{p}_{k+1}$  close to  $\mathcal{C}$ . In addition, for each iterate  $\mathbf{p}_k$  that we actually want to use as waypoint for motion planning (some iterates could be skipped), since (28) represents rigidity constraints, we can enforce feasibility by computing for each robot the pose minimizing the distance between the desired and achievable tag locations, in a least-squares sense (this corresponds to a standard pose estimation problem [48, Section 8.1]).

A local convergence result for the iterations (32) to a local constrained minimum  $\mathbf{p}^*$  and Lagrange multiplier  $\boldsymbol{\lambda}^*$  is stated in [47, Proposition 5.4.2], for constant stepsizes  $\eta_k = \delta$ ,  $k \geq 0$ , and  $\delta$  sufficiently small. Note that this method is not guaranteed to converge starting from any initial configuration  $\mathbf{p}_0$ . Hence, it may need to be combined with or replaced by other

optimization methods with global convergence guarantees, such as multiplier methods, as discussed in [47, Section 5.2]. We refer the reader to the literature on nonlinear programming for further discussion and comparison of available iterative methods, and focus instead in the rest of this section on the computation of the derivatives  $\partial J_c / \partial \mathbf{p}$  and  $\partial \mathbf{f}_c / \partial \mathbf{p}$  appearing in (32), which are required for the implementation of all such methods. We specialize the discussion above to the deployment problem where some robots carry multiple tags, which requires evaluating the cost function (31) and its gradient. First, we only take into account in the CRLB the constraints on the distances between the intra-robot tags, since this leads to somewhat simpler expressions and computations. In Section VI-C, we include in the CRLB the full information about the relative positions of these tags.

### B. CRLB with Distance Constraints

Considering Fig. 2, as robots carrying multiple tags move, their tags' relative positions must satisfy rigid displacement constraints. We partition the set of tags  $\mathcal{U}$  into  $R$  groups  $\mathcal{U}_1, \dots, \mathcal{U}_R$ , with  $\sum_{r=1}^R |\mathcal{U}_r| = U$ , such that the tags in group  $\mathcal{U}_r$  are rigidly connected (mounted on the same robot). To simplify the discussion in the following, we assume that each group has  $|\mathcal{U}_r| \geq n$  tags in dimension  $n$  and that these tags are in general position (no 3 tags aligned, and no 4 tags coplanar in dimension 3). As a result, each group of tags forms an infinitesimally rigid framework for the complete graph (note that all pairwise distances within a group  $\mathcal{U}_r$  are known). For example, we can simply have 2 tags on each robot if  $n = 2$ , or 3 non-aligned tags if  $n = 3$ . We also ignore the possibility of having known rigid constraints between anchors and tags. The analysis can be extended to mixed networks of robots carrying a single or multiple tags, or both anchors and tags, in a straightforward manner.

Since we know the relative positions of the tags in  $\mathcal{U}_r$  in the robot's frame of reference (by carefully placing them on the robot), this information should in principle be included in the CRLB. First, however, we only include the information about relative *distances* between tags in each group, as this leads to simpler algorithms. In this case, in the framework of Section VI-A,  $\mathbf{f}_c$  has one component for each pair of tags  $\{i, j\}$  in the same group  $\mathcal{U}_r$ , of the form

$$\mathbf{f}_c^{\{i,j\}}(\mathbf{p}_U) = \|\mathbf{p}_{ij}\|^2 - d_{ij}^2,$$

where  $d_{ij}$  is perfectly known. If we order these components by listing all pairs of tags in the same set  $\mathcal{U}_1, \mathcal{U}_2, \dots, \mathcal{U}_R$ , then we obtain for the Jacobian matrix

$$\frac{\partial \mathbf{f}_c(\mathbf{p}_U)}{\partial \mathbf{p}_U} = \text{diag}(\mathbf{R}_1, \dots, \mathbf{R}_R), \quad (33)$$

where  $\mathbf{R}_r$  is the rigidity matrix defined in Section IV-A, for the framework formed by a complete graph among the tags in group  $\mathcal{U}_r$ . Because the framework within each group is infinitesimally rigid, the kernel of each matrix  $\mathbf{R}_r$  is spanned by three explicitly known vectors if  $n = 2$ , or six if  $n = 3$ , as described in Proposition 2. Then we can compute the matrix  $\mathbf{A}_U = [\mathbf{A}_1 \ \dots \ \mathbf{A}_R]$  with  $nU$  rows and  $3R$  (if  $n = 2$ ) or  $6R$  (if  $n = 3$ ) columns spanning the kernel of (33). For

example, based on the discussion above Proposition 2, if  $n = 2$  we can take  $\mathbf{A}_r = [\mathbf{v}_{T_x}^r \ \mathbf{v}_{T_y}^r \ \mathbf{v}_{R_z}^r]$ , with  $[\mathbf{v}_{T_x}^r]_{2i-1} = 1$ ,  $[\mathbf{v}_{T_y}^r]_{2i} = 1$ ,  $[\mathbf{v}_{R_z}^r]_{2i-1} = -y_i$  and  $[\mathbf{v}_{R_z}^r]_{2i} = x_i$  for all  $i \in \mathcal{U}_r$  and zeros everywhere else. From these explicit expressions of  $\mathbf{A}_U$ , we can also immediately compute the derivatives  $\partial \mathbf{A}_U / \partial \xi_i$ , for  $\xi_i \in \{x_i, y_i, z_i\}$ .

Since determining  $\mathbf{A}_U(\mathbf{p}_U)$  allows us to compute  $J_c(\mathbf{p}_U)$  using (30), the only missing element to execute the iterations (32) is the gradient of  $J_c$ . For simplicity, suppose that  $\mathbf{F}_c := \mathbf{A}_U^T \mathbf{F}_U \mathbf{A}_U$  is invertible. Since  $\mathbf{A}_U$  can be taken to be full column rank, this can be ensured by fulfilling the assumptions of Theorem 2, guaranteeing that  $\mathbf{F}_U$  is invertible. Then, we have

$$\begin{aligned} \frac{\partial J_c}{\partial \xi_i} &= \frac{\partial}{\partial \xi_i} \text{Tr} \{ \mathbf{A}_U \mathbf{F}_c^{-1} \mathbf{A}_U^T \} \\ &= 2 \text{Tr} \left\{ \mathbf{F}_c^{-1} \mathbf{A}_U^T \frac{\partial \mathbf{A}_U}{\partial \xi_i} \right\} - \text{Tr} \left\{ \mathbf{A}_U \mathbf{F}_c^{-1} \frac{\partial \mathbf{F}_c}{\partial \xi_i} \mathbf{F}_c^{-1} \mathbf{A}_U^T \right\} \\ &= 2 \text{Tr} \left\{ \mathbf{F}_c^{-1} \mathbf{A}_U^T (\mathbf{I} - \mathbf{B}_U \mathbf{F}_U) \frac{\partial \mathbf{A}_U}{\partial \xi_i} \right\} - \text{Tr} \left\{ \mathbf{B}_U^2 \frac{\partial \mathbf{F}_U}{\partial \xi_i} \right\}. \end{aligned} \quad (34)$$

### C. CRLB with Constrained Relative Positions

When we place two tags  $i$  and  $j$  on a robot  $r$ , we can in fact know the relative positions (RP)  $\mathbf{p}_{ij}^r$  of these tags in the frame of robot  $r$ , not just their distance. Since a position estimator can leverage this information to improve its accuracy, we derive in this section the corresponding CRLB. To simplify the presentation, we assume here that each robot carries at least two tags.

To obtain the CRLB, let us first introduce  $R$  new parameters  $\boldsymbol{\theta} := \text{col}(\boldsymbol{\theta}_1, \dots, \boldsymbol{\theta}_R)$ , one for each robot, where  $\boldsymbol{\theta}_i \in \mathbb{R}^q$ , with  $q = 1$  if  $n = 2$  and  $q = 3$  if  $n = 3$ . Then, for the extended set of parameters  $\tilde{\mathbf{p}}_U = (\mathbf{p}_U, \boldsymbol{\theta})$  and the measurements (1) or (2), we denote the extended FIM

$$\tilde{\mathbf{F}}_U = -\mathbb{E} \left\{ \frac{\partial^2 \ln f(\tilde{\mathbf{d}}; \tilde{\mathbf{p}}_U)}{\partial \tilde{\mathbf{p}}_U \partial \tilde{\mathbf{p}}_U^T} \right\} = \begin{bmatrix} \mathbf{F}_U & \mathbf{0}_{nU, qR} \\ \mathbf{0}_{qR, nU} & \mathbf{0}_{qR, qR} \end{bmatrix}. \quad (35)$$

In the following, we add constraints between the tag positions and the parameters  $\boldsymbol{\theta}$ , in such a way that the latter represent the robot orientations in exponential coordinates. Then, we compute the constrained FIM from  $\tilde{\mathbf{F}}_U$  using Theorem 1 to obtain the final CRLB on position estimates.

It is convenient to number and order the tags as follows. Consider robot  $r \in \{1, \dots, R\}$  and associated tags  $\mathcal{U}_r$ , using the notation of Section VI-B. Pick one tag in  $\mathcal{U}_r$ , denoted in the following  $1^r$ . The other tags of  $\mathcal{U}_r$  are denoted  $2^r, \dots, U_r^r$ , with  $U_r = |\mathcal{U}_r|$ . We group these latter tags by robot and list them in the order

$$\mathbf{p}_o := \text{col}(\mathbf{p}_{2^1}, \dots, \mathbf{p}_{U_1^1}, \dots, \mathbf{p}_{2^R}, \dots, \mathbf{p}_{U_R^R}) \in \mathbb{R}^{n(U-R)}, \quad (36)$$

from robot 1 to robot  $R$ . The positions of the  $R$  tags  $1^r$  are also grouped in the vector

$$\mathbf{p}_c := \text{col}(\mathbf{p}_{1^1}, \dots, \mathbf{p}_{1^R}) \in \mathbb{R}^{nR}.$$

Then, we have  $\tilde{\mathbf{p}}_U = \text{col}(\mathbf{p}_o, \mathbf{p}_c, \boldsymbol{\theta})$ .

Next, for each tag  $j^r \in \mathcal{U}_r$  other than  $1^r$ , we add the constraint  $\mathbf{f}^{(r,j^r)}(\mathbf{p}_{1^r}, \mathbf{p}_{j^r}, \boldsymbol{\theta}_r) = \mathbf{0} \in \mathbb{R}^n$ , where

$$\mathbf{f}^{(r,j^r)}(\mathbf{p}_{1^r}, \mathbf{p}_{j^r}, \boldsymbol{\theta}_r) = \mathbf{p}_{j^r} - \mathbf{p}_{1^r} - \exp([\boldsymbol{\theta}_r]_{\times}) \mathbf{p}_{j^r}^{1^r}, \quad (37)$$

with the notation (depending if  $n = 2$  or  $n = 3$ )

$$[\theta]_{\times} = \begin{bmatrix} 0 & -\theta \\ \theta & 0 \end{bmatrix}, \text{ if } \theta \in \mathbb{R},$$

$$[\theta]_{\times} = \begin{bmatrix} 0 & -\theta_z & \theta_y \\ \theta_z & 0 & -\theta_x \\ -\theta_y & \theta_x & 0 \end{bmatrix}, \text{ if } \theta = [\theta_x, \theta_y, \theta_z]^T \in \mathbb{R}^3.$$

There are  $U_r - 1$  constraints of the form (37) for robot  $r$ , each of dimension  $n$ , which represent a change from the known coordinates  $\mathbf{p}_{j^r 1^r}^r$  in the robot frame to the (unknown) coordinates  $\mathbf{p}_{j^r 1^r}$  in the world frame  $\mathfrak{F}$ , with the matrix  $\exp([\theta_r]_{\times})$  representing the rotation matrix from  $\mathfrak{F}$  to the frame of robot  $r$ , using the exponential coordinate representation [49]. Define in the following the notation  $\exp([\theta_r]_{\times}) := \mathbf{R}_{\theta_r}$  and

$$\Phi_{\theta_r}^{(r,j^r)} := \mathbf{R}_{\theta_r} \mathbf{p}_{j^r 1^r}^r, \quad \text{for } j^r \in \mathcal{U}_r, 1 \leq r \leq R.$$

**Remark 9.** Recall that when  $n = 2$ , we have simply

$$\exp([\theta]_{\times}) = \begin{bmatrix} \cos(\theta) & -\sin(\theta) \\ \sin(\theta) & \cos(\theta) \end{bmatrix},$$

and when  $n = 3$ ,  $\exp([\theta]_{\times})$  can be computed efficiently using Rodrigues' formula [49, Proposition 3.1].

Considering (37) for all  $R$  robots, we obtain  $U - R$  constraints on the parameters  $\tilde{\mathbf{p}}_{\mathcal{U}}$ , each of dimension  $n$ . We list these constraints in the same order as for  $\mathbf{p}_o$  in (36) and denote them  $\mathbf{f}_{\text{RP}}(\mathbf{p}_o, \mathbf{p}_c, \theta) = \mathbf{0}$ . For the constrained CRLB, we are interested in the kernel of the Jacobian matrix of  $\mathbf{f}_{\text{RP}}$ . Remark that with the chosen ordering of tags and constraints, we have  $\frac{\partial \mathbf{f}_{\text{RP}}}{\partial \mathbf{p}_o} = \mathbf{I}_{n(U-R)}$ . If we define

$$\mathbf{N} := \begin{bmatrix} \frac{\partial \mathbf{f}_{\text{RP}}}{\partial \mathbf{p}_c} & \frac{\partial \mathbf{f}_{\text{RP}}}{\partial \theta} \end{bmatrix}, \quad (38)$$

and  $\mathbf{A}_{\text{RP}} := \text{span} \left\{ \ker \frac{\partial \mathbf{f}_{\text{RP}}}{\partial \tilde{\mathbf{p}}_{\mathcal{U}}} \right\}$ , then immediately

$$\begin{aligned} \mathbf{A}_{\text{RP}} &= \text{span} \left\{ \ker \begin{bmatrix} \mathbf{I}_{n(U-R)} & \mathbf{N} \end{bmatrix} \right\} \\ &= \text{col}(-\mathbf{N}, \mathbf{I}_{(n+q)R}). \end{aligned} \quad (39)$$

Indeed,  $\frac{\partial \mathbf{f}_{\text{RP}}}{\partial \tilde{\mathbf{p}}_{\mathcal{U}}}$  is of rank  $n(U - R)$ , so  $\mathbf{A}_{\text{RP}}$  should have  $nU + qR - n(U - R) = (n + q)R$  independent columns, and clearly

$$\frac{\partial \mathbf{f}_{\text{RP}}}{\partial \tilde{\mathbf{p}}_{\mathcal{U}}} \mathbf{A}_{\text{RP}} = -\mathbf{N} + \mathbf{N} = \mathbf{0}.$$

Hence, it is sufficient to compute  $\mathbf{N}$  to obtain  $\mathbf{A}_{\text{RP}}$ .

**Proposition 6.** The matrix  $\mathbf{N}$  in (38) is defined by

$$\mathbf{N} = \text{col} \left( \left\{ \mathbf{N}^{(r,j^r)} \right\}_{1 \leq r \leq R, 2^r \leq j^r \leq U^r} \right) \in \mathbb{R}^{n(U-R) \times (n+q)R}.$$

where the blocks  $\mathbf{N}^{(r,j^r)} \in \mathbb{R}^{n \times (n+q)R}$  are stacked in the same order as  $\mathbf{p}_o$  in (36) and are of the form

$$\mathbf{N}^{(r,j^r)} = - \begin{bmatrix} \mathbf{0}_{n,n(r-1)} & \mathbf{I}_n & \mathbf{0}_{n,s} & \mathbf{N}_{\theta_r}^{(r,j^r)} & \mathbf{0}_{n,(R-r)q} \end{bmatrix}$$

with  $s = (R - r)n + (r - 1)q$ , where

$$\mathbf{N}_{\theta_r}^{(r,j^r)} = \begin{cases} [1]_{\times} \Phi_{\theta_r}^{(r,j^r)} \in \mathbb{R}^2 & \text{if } n = 2, \\ \left[ \Phi_{\theta_r}^{(r,j^r)} \right]_{\times} \Omega_{\theta_r} \in \mathbb{R}^{3 \times 3} & \text{if } n = 3, \end{cases} \quad (40)$$

with  $\Omega_{\theta_r} := (\theta_r \theta_r^{\top} + (\mathbf{I}_3 - \mathbf{R}_{\theta_r})[\theta_r]_{\times}) \|\theta_r\|^{-2}$ .

*Proof.* Decompose  $\mathbf{N}^{(r,j^r)}$  by blocks

$$\mathbf{N}^{(r,j^r)} = \begin{bmatrix} \mathbf{G}_1 & \dots & \mathbf{G}_R & \mathbf{H}_1 & \dots & \mathbf{H}_R \end{bmatrix}$$

with  $\mathbf{G}_i \in \mathbb{R}^{n \times n}$  and  $\mathbf{H}_i \in \mathbb{R}^{n \times q}$ . The matrix  $\mathbf{N}^{(r,j^r)}$  is obtained by taking the partial derivatives of  $\mathbf{f}^{(r,j^r)}$  in (37) with respect to the coordinates of  $\mathbf{p}_{1^r}$ , which gives the block  $\mathbf{G}_r = -\mathbf{I}_n$ , and with respect to the coordinates of  $\theta_r$ , which gives the block  $\mathbf{H}_r = -\mathbf{N}_{\theta_r}^{(r,j^r)} \in \mathbb{R}^{n \times q}$ . All other blocks are zero. The expression of  $\mathbf{H}_r$  comes from the fact that  $[\theta_r]_{\times} = \theta_r [1]_{\times}$  when  $n = 2$ , whereas when  $n = 3$ , we have

$$\frac{\partial \Phi_{\theta_r}^{(r,j^r)}}{\partial \theta_r} = -\mathbf{R}_{\theta_r} [\mathbf{p}_{j^r 1^r}^r]_{\times} \frac{\theta_r \theta_r^{\top} + (\mathbf{R}_{\theta_r}^{\top} - \mathbf{I}_3)[\theta_r]_{\times}}{\|\theta_r\|^2}$$

from [50, Result 1]. This expression is further reduced to the one in (40) using elementary properties of rotation matrices.  $\square$

With the matrices  $\tilde{\mathbf{F}}_{\mathcal{U}}$  and  $\mathbf{A}_{\text{RP}}$  defined in (35) and (39), we can follow the discussion of Section VI-A and define  $\mathbf{B}_{\text{RP}} := \mathbf{A}_{\text{RP}} [\mathbf{A}_{\text{RP}}^{\top} \tilde{\mathbf{F}}_{\mathcal{U}} \mathbf{A}_{\text{RP}}]^{\dagger} \mathbf{A}_{\text{RP}}^{\top}$  to obtain a CRLB taking the RP constraints into account. We can build a cost function providing a lower bound on MSE of the tag positions as

$$J_c(\mathbf{p}) = \text{Tr} \left\{ \mathbf{C} \mathbf{B}_{\text{RP}} \mathbf{C}^{\top} \right\}, \quad (41)$$

similarly to (31), where  $\mathbf{C} = [\mathbf{I}_{nU} \ \mathbf{0}_{nU,qR}]$  is introduced here to select the  $nU \times nU$  first block of  $\mathbf{B}_{\text{RP}}$  and hence consider only the uncertainty in the estimate  $\tilde{\mathbf{p}}_{\mathcal{U}}$ . Alternatively, the uncertainty in the estimate of the whole extended state  $\tilde{\mathbf{p}}_{\mathcal{U}}$  can be considered by using the matrix  $\mathbf{C} = \text{diag}(\mathbf{I}_{nU}, w_{\theta} \mathbf{I}_{qR})$ , with  $w_{\theta}$  a weight to select. To compute the gradient with respect to  $\mathbf{p}$  for (32), similarly to (34), we have, for  $\xi \in \{x, y, z\}$ :

$$\frac{\partial J_c}{\partial \xi_i} = 2 \text{Tr} \left\{ \mathbf{C} \frac{\partial \mathbf{A}_{\text{RP}}}{\partial \xi_i} \mathbf{D}^{\top} \right\} - \text{Tr} \left\{ \mathbf{D} \frac{\partial \mathbf{F}_c}{\partial \xi_i} \mathbf{D}^{\top} \right\}, \quad (42)$$

with  $\mathbf{D} := \mathbf{C} \mathbf{A}_{\text{RP}} \mathbf{F}_c^{-1}$ , assuming  $\mathbf{F}_c = \mathbf{A}_{\text{RP}}^{\top} \tilde{\mathbf{F}}_{\mathcal{U}} \mathbf{A}_{\text{RP}}$  to be invertible. To compute the derivative  $\partial \mathbf{A}_{\text{RP}} / \partial \xi_i$ , it is sufficient to know how to compute the terms  $\partial \mathbf{N}_{\theta_r}^{(r,j^r)} / \partial \xi_i$ . Then, noting that  $\Phi_{\theta_r}^{(r,j^r)} = \mathbf{p}_{j^r} - \mathbf{p}_{1^r}$ , the differentiation of (40) yields

$$\frac{\partial \mathbf{N}_{\theta_r}^{(r,j^r)}}{\partial \xi_i} = \begin{cases} [1]_{\times} \mathbf{e}_{\xi} \psi_{j^r}(i) & \text{if } n = 2; \\ [\mathbf{e}_{\xi}]_{\times} \Omega_{\theta_r} \psi_{j^r}(i) & \text{if } n = 3, \end{cases}$$

for  $\xi \in \{x, y, z\}$ , where  $\mathbf{e}_x, \mathbf{e}_y, \mathbf{e}_z$  forms the canonical basis of  $\mathbb{R}^3$ , and we introduced the notation  $\psi_{j^r}(i)$  equals to 1 if  $i = j^r$ , to  $-1$  if  $i = 1^r$  and to zero otherwise.

## VII. SIMULATIONS

In this section, we present simulation results for two deployment scenarios. The first scenario is a structure inspection problem by a multi-robot network maintaining localizability while the task is performed. The second concerns the deployment of an Unmanned Ground Vehicle (UGV) carrying several tags, where we include the distance and relative position constraints in the CRLB-based potential.

### A. Cooperative Structure Inspection

Consider a system composed of  $N = 16$  agents, with  $U = 12$  tags carried by mobile robots (i.e.,  $\mathcal{U} = \{1, \dots, 12\}$ ) and  $K = 4$  fixed anchors with known positions (i.e.,  $\mathcal{K} = \{13, \dots, 16\}$ ). Each robot carries an UWB transceiver to communicate and take ranging measurements with any other robot or UWB anchor, following the model (1), via a Two Way Ranging (TWR) protocol [51], [52].

We assign an inspection task to the two first robot-tags 1 and 2, called “leaders”, while the remaining robot-tags  $\mathcal{U}_F = \{i \in \mathcal{U}, i > 2\}$  are called “followers” and deploy to support accurate localization. The leaders are required to visit ten waypoints each, underneath a  $50 \text{ m} \times 10 \text{ m}$  rectangular structure represented in blue in Fig. 3, in order to inspect it. The links in the ranging/communication network are represented on Fig. 3 by the sparsity pattern of the network adjacency matrix, i.e., showing its non-zero entries. In particular, we stress that the leaders cannot communicate directly with the anchors.

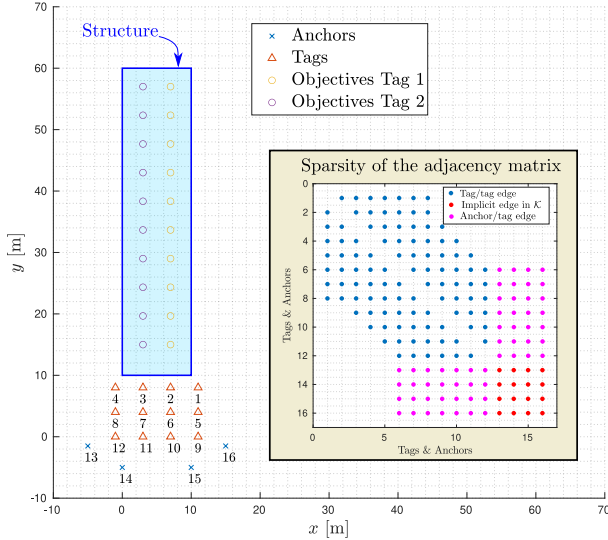


Fig. 3: Initial system configuration, waypoints for the leaders 1 et 2 and ranging network sparsity.

1) *Motion Planner for the Follower Robots:* We follow the motion planning framework based on artificial potentials presented in Section II. To enhance the localizability of the robots, we chose to include in the overall potential the cost  $J_D(\mathbf{p}) = -\log \det \mathbf{F}_U$  introduced in Section III. This choice is motivated in particular by the fact that in a decentralized system, computing the gradient of  $J_D$  via Algorithm 1 requires a single distributed matrix inversion. We add safety margins between robots by introducing a collision avoidance potential

$$J_{\text{avd}}(\mathbf{p}) = \frac{1}{2} \sum_{i \in \mathcal{U}} \sum_{j \in \mathcal{U} \cup \mathcal{K}} (d_{ij}^{-1} - d_a^{-1})^2 \mathbf{1}_{d_{ij} < d_a}.$$

We also encourage ranging tags to maintain proximity, in order to limit the potential deterioration of ranging measurements at

long distances, e.g., due to power fading. To do so, we use the potential

$$J_{\text{con}}(\mathbf{p}) = \frac{1}{2} \sum_{i \in \mathcal{U}} \sum_{j \in \mathcal{N}_i} (d_{ij} - d_c)^2 \mathbf{1}_{d_{ij} > d_c}.$$

In our simulations, we set  $d_a = 2 \text{ m}$  and  $d_c = 50 \text{ m}$ .

Therefore, the overall potential is defined as  $J(\mathbf{p}) := K_l J_D(\mathbf{p}) + K_c J_{\text{con}}(\mathbf{p}) + K_a J_{\text{avd}}(\mathbf{p})$  where  $K_l, K_a, K_c > 0$  are constant parameters. The leaders travel directly to their prespecified waypoints. Meanwhile, each follower  $i \in \mathcal{U}_F$  implements the following gradient descent scheme

$$\mathbf{p}_{i,k+1}^d = \hat{\mathbf{p}}_{i,k} - \frac{\partial J(\hat{\mathbf{p}}_{\mathcal{U},k})}{\partial \mathbf{p}_{i,k}} \times \min \left\{ 1, \frac{\Delta_{\text{vel}}}{\|\partial J / \partial \mathbf{p}_{i,k}\|} \right\}, \quad (43)$$

i.e., with robot  $i$  at its current position  $\mathbf{p}_{i,k}$  at period  $k \geq 0$ , a gradient step provides the next desired position  $\mathbf{p}_{i,k+1}^d$ . The min term bounds the stepsizes so that  $\|\mathbf{p}_{i,k+1}^d - \mathbf{p}_{i,k}\| \leq \Delta_{\text{vel}}$ , for some specified value of  $\Delta_{\text{vel}}$ . For  $\xi_i \in \{x_i, y_i\}$ , we compute  $\partial J_D / \partial \xi_i$  by (17), possibly using Richardson iterations presented in Algorithm 1 for a decentralized implementation. The expressions of the derivatives  $\partial J_{\text{con}} / \partial \xi_i$  and  $\partial J_{\text{avd}} / \partial \xi_i$  of the other potentials are standard [49] and can be distributively computed since they only depend on each tag’s neighborhood. Note that in (43) we do not assume that the true positions are accessible but compute the gradients at the estimates  $\hat{\mathbf{p}}_{i,k}$  (see (46)).

The gradient descent scheme is used to obtain desired waypoints for the tags, which we can track using controllers on the robots. For concreteness, assume that all robots are identical with unicycle kinematics [53, Chap. 4]

$$\dot{x}_M = v \cos(\theta), \quad \dot{y}_M = v \sin(\theta), \quad \dot{\theta} = \omega \quad (44)$$

where  $\omega$  and  $v$  are the rotational and translational velocities and  $\theta$  is the robot’s heading with respect to  $\mathfrak{F}$ . The coordinates of the tag in the robot’s frame (for any  $i$ ) are  $\mathbf{p}_i^r = [a, b]^\top$ , with  $a \neq 0$ , see Fig. 4. With  $\dot{\mathbf{p}}_i \in \mathbb{R}^2$  the velocity of tag  $i$  in  $\mathfrak{F}$ , implementing the following Proportional-Integral (PI) controller

$$\dot{\mathbf{p}}_i = K_P(\mathbf{p}_i^d(t) - \mathbf{p}_i(t)) + K_I \int_{\tau=0}^t (\mathbf{p}_i^d(\tau) - \mathbf{p}_i(\tau)) d\tau, \quad (45)$$

with  $K_P, K_I > 0$ , allows the tags to track the desired (piecewise constant) trajectory  $\mathbf{p}^d$ . This corresponds to a velocity command  $\mathbf{u}_i := [v_i, \omega_i]^\top$  for robot  $i$ , since  $\mathbf{u}_i = \mathbf{T}(\theta_i) \dot{\mathbf{p}}_i$  [49, Section 13.3.1.4] with

$$\mathbf{T}(\theta) = \frac{1}{a} \begin{bmatrix} a \cos \theta - b \sin \theta & a \sin \theta + b \cos \theta \\ -\sin \theta & \cos \theta \end{bmatrix}.$$

2) *Simulation and Performance Analysis:* We choose the weights in the potential  $J$  as  $K_l = 5 \times 10^4$ ,  $K_a = K_c = 1 \times 10^3$  and the maximal step length  $\Delta_{\text{vel}} = 2 \text{ m}$ . When the leaders reach their  $o$ -th waypoint, we repeat the iterations (43)  $N_{\text{iter}} = 30$  times to compute sufficiently distant waypoints for the followers. Then, we only transmit the desired position  $\mathbf{p}_{i,oN_{\text{iter}}}^d$  to the controller of each follower  $i \in \mathcal{U}_F$  in order to enhance the tags’ localizability. The tags are positioned on the robots so that  $a = b = 0.5 \text{ m}$ , and the PI controller gains are

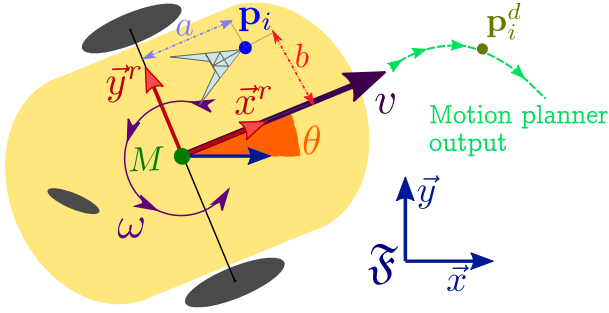


Fig. 4: Robot and tag configuration for trajectory tracking.  $(M, \bar{x}^r, \bar{y}^r)$  is the robot frame.

$K_p = 3$ ,  $K_i = 0.5$ . The controller (45) follows the trajectory computed from (43) with a maximum tracking error of about 10 cm.

To illustrate the performance of our deployment scheme we perform  $M = 1000$  Monte Carlo simulations, using the measurement model (1) with  $\sigma = 5$  cm. At simulation  $\rho$ , the position estimates  $\hat{\mathbf{p}}_{\mathcal{U},k}^\rho$  used in (43) are obtained by solving the least-squares problem

$$\hat{\mathbf{p}}_{\mathcal{U},k}^\rho = \underset{\mathbf{p}_{\mathcal{U}} \in \mathbb{R}^{2U}}{\operatorname{argmin}} Q(\mathbf{p}_{\mathcal{U}}),$$

$$\text{with } Q(\mathbf{p}_{\mathcal{U}}) := \sum_{i \in \mathcal{U}} \sum_{j \in \mathcal{N}_i} (\|\mathbf{p}_{i,k} - \mathbf{p}_{j,k}\| - \tilde{d}_{ij,k}^\rho)^2, \quad (46)$$

where  $\mathbf{p}_{j,k}$  is the anchor position in (46) if  $j \in \mathcal{K}$  and  $\tilde{d}_{ij,k}^\rho$  are the range measurements.

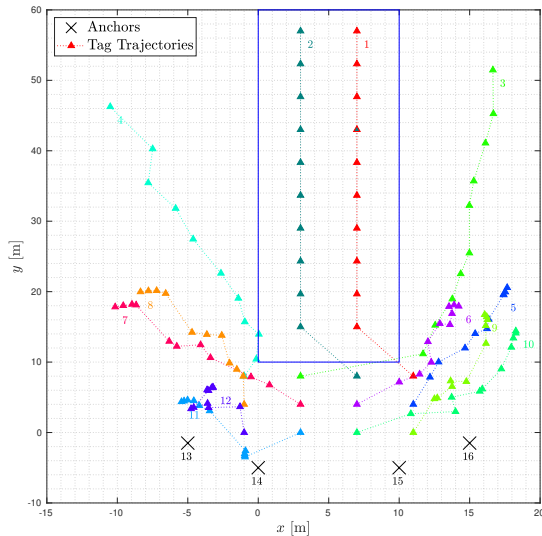


Fig. 5: Tag trajectories in the workspace.

As shown by the trajectories on Fig. 5, the leaders follow their assigned paths and the followers maintain the network's localizability. Initially, all robots are aligned, a geometry with poor localizability. On Fig. 6, we plot the empirical average  $\bar{J}_D$  and  $3\sigma$  confidence bounds (CBs) for the potential  $J_D$  over the  $M$  simulations. Initially, the localizability potential

decreases as the followers deploy. The following step increases occur when the leaders move to their next waypoints and the network extends, while the anchors remain fixed and far away, see Fig. 5. Overall however, the followers manage to keep the localizability at a low value. For comparison, we plot in blue on Fig. 6 the evolution of the localizability potential without deployment of the followers. We also plot the empirical statistical entropy  $\ln \det \hat{\Sigma}_k$  and its CBs, with  $\hat{\Sigma}_k$  the empirical covariance of the estimates  $\hat{\mathbf{p}}_{\mathcal{U},k}$  obtained by solving (46). The plot highlights that the entropy remains close to the theoretical lower bound provided by  $J_D$ , as discussed in Section III-B.

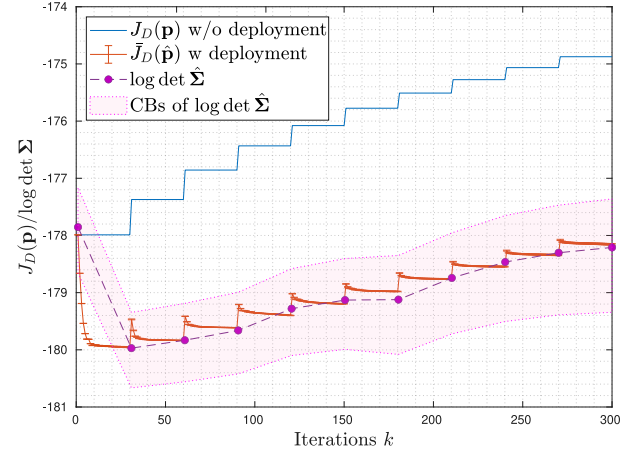


Fig. 6: Localizability potential with and without follower deployment, empirical entropy and  $3\sigma$  confidence bounds obtained from the Monte-Carlo simulations. The leaders' waypoints are updated every  $N_{\text{iter}} = 30$  iterations of the gradient descent scheme.

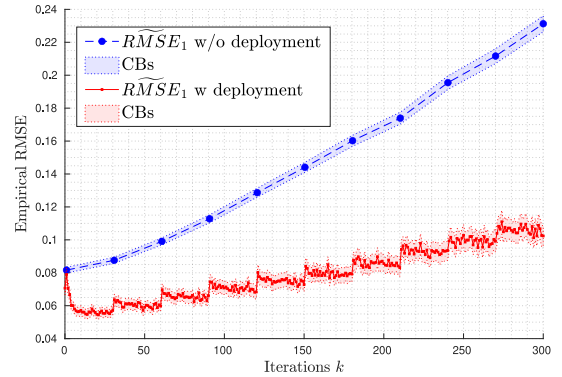


Fig. 7: Plot of the empirical RMSE over the trajectory.

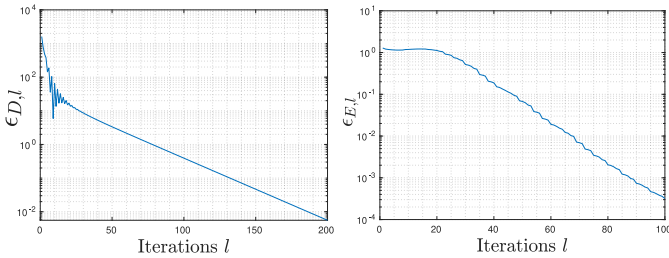
Even though the deployment is performed here using  $J_D$  to measure localizability, which is related to entropy, Fig. 7 shows that other localization accuracy measures are improved as well. In this case, we plot the empirical Root Mean Squared Error (RMSE) for the location estimate of the first leader tag, the plot for the second leader being similar. Namely, at each iteration  $k$  of (43), we compute the empirical MSE  $\widehat{MSE}_{1,k} := \frac{1}{M} \sum_{\rho=1}^M \|\hat{\mathbf{p}}_{1,k}^\rho - \mathbf{p}_{1,k}\|^2$ , with  $\hat{\mathbf{p}}_{1,k}^\rho$  the estimate of  $\mathbf{p}_{1,k}$  for simulation  $\rho$ . Then  $RMSE_1 :=$

$(\widetilde{MSE}_{1,k})^{1/2}$ . The CBs shown on Fig. 7 are defined by  $b_{\pm,k} = s_{\pm,k}^{1/2}$ , where  $s_{\pm,k} = \widetilde{MSE}_{1,k} \pm 3\widetilde{\sigma}_{1,k}/\sqrt{M}$ , with  $\widetilde{\sigma}_{1,k}^2 = \frac{1}{M-1} \sum_{\rho=1}^M [\|\hat{\mathbf{p}}_{1,k}^\rho - \mathbf{p}_{1,k}\|^2 - \widetilde{MSE}_{1,k}]^2$  the empirical variance of the samples. For comparison, we also plot  $\widetilde{RMSE}_1$  without deployment. The empirical RMSE is significantly reduced by the motion of the followers, remaining below 12 cm even when the leader 1 is at its farthest waypoint.

3) *Distributed Gradient Computations*: Here we illustrate the convergence of the distributed algorithms of Section V estimating the gradients of the localizability potentials, more specifically Algorithm 1 (D-Opt) and Algorithm 2 (E-Opt). Define the relative error  $\epsilon_{S,l}$  on the gradients at the  $l$ -th iteration as follows

$$\epsilon_{S,l} = \frac{\|\widehat{[\partial J_S / \partial \mathbf{p}_U]}_l - \partial J_S / \partial \mathbf{p}_U\|_2}{\|\partial J_S / \partial \mathbf{p}_U\|_2}$$

for each scheme  $S \in \{D, E\}$  producing the estimates  $\widehat{[\partial J_S / \partial \mathbf{p}_U]}_l$ . On Fig. 8 we plot the errors  $\epsilon_{E,l}$  and  $\epsilon_{D,l}$  for increasing values of  $l$  at the last (fixed) configuration  $\mathbf{p}_U$  of the trajectory shown on Fig. 5. For the D-Opt scheme, we arbitrarily choose the initial condition  $\mathbf{x}_0 = \mathbf{I}_{n \times u}$  in Algorithm 1, which is far from the ideal value  $\mathbf{F}_U^{-1}$ . Nonetheless, an error of 10% on the gradient is obtained after about 120 iterations. To estimate the gradient of  $J_E$ , we arbitrarily set  $\mathbf{w}(0) = \mathbf{1}_{nU}$  in Algorithm 2. In this case a relative error of 10% is obtained after 50 iterations, with the inner loop to compute the squared norm of the eigenvector set to  $\tilde{n}_{iter} = 10$ .



(a) Errors on D-Opt gradient. (b) Errors on E-Opt gradient.  
Fig. 8: Convergence of the D-Opt and E-Opt gradient estimates for the last configuration in the trajectory.

The convergence speed of both algorithm depends on the structure of  $\mathbf{F}_U$  and the chosen initial condition. In practice, for  $k = 0$  we can initialize the decentralized gradient estimation schemes with arbitrary values and wait for a sufficient number of iterations, until some stopping condition of the form  $\max_{i \in U} \|\widehat{[\partial J_S / \partial \mathbf{p}_i]}_l - \widehat{[\partial J_S / \partial \mathbf{p}_i]}_{l-1}\| < \epsilon$  is reached, for some tolerance threshold  $\epsilon > 0$ . Then, for the next periods  $k > 0$  of the trajectory, we can use for initialization the values obtained after convergence at the end of the previous period  $k - 1$ , which should lead to faster convergence.

### B. Deployment of a UGV Carrying Several Anchors

Here we illustrate the results of Section VI and the performance difference between leveraging information only on relative distances or on the full relative positions. Consider the robot shown in Fig. 9, following the kinematic model

(44) and carrying two tags  $\mathcal{U} = \{1, 2\}$  placed at positions  $\mathbf{p}_1^r = [1, 0]^\top$  and  $\mathbf{p}_2^r = [-1, 0]^\top$  in the robot frame, centered at  $\mathbf{p}_M = \frac{1}{2}(\mathbf{p}_1 + \mathbf{p}_2)$ . Three fixed anchors  $\mathcal{K} = \{3, 4, 5\}$  are placed at the coordinates  $\mathbf{p}_3 = [-5, 5]^\top$ ,  $\mathbf{p}_4 = [5, -5]^\top$  and  $\mathbf{p}_5 = [5, 5]^\top$  in the absolute frame. All nodes communicate and obtain range measurements with each other, following the Gaussian additive model (1) with  $\sigma = 0.1$  m. The heading of the robot is  $\theta$  and  $\exp[\theta]_\times$  is the rotation matrix between  $\mathcal{F}$  and the robot frame.

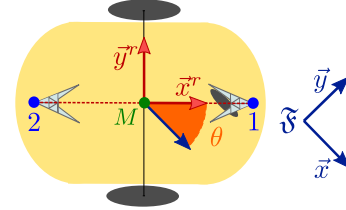


Fig. 9: Robot equipped with two tags.

In scenario (D), we include the constraint  $d_{12} = 2$  m as in Section VI-B, and define the cost function as (31). In scenario (RP), we include the constraint  $\mathbf{p}_{12}^r = [2, 0]^\top$  as in Section VI-C and define the cost function as (41), so that it can be compared to the previous one. We compute the potentials and their derivatives with the results of Section VI and implement the scheme (32) to compute a sequence of desired poses. The robot reaches them by using the pose controller presented in [54], which includes heading control, in contrast to (45). At  $k = 0$ , the initial configuration of the robot in both cases is given by  $\mathbf{p}_M(0) = [-15, -4]^\top$  and  $\theta(0) = -\pi/8$ . The cost and robot trajectories are shown in Fig. 10, denoting  $F = 5000$  the last iteration index of (32). Thanks to the dual penalization of the rigidity constraint, the steady state configuration of the tags provided by (32) is feasible for the robot.

The following constrained least-squares estimators  $\hat{\mathbf{p}}_U^D$  and  $\hat{\mathbf{p}}_U^{RP}$  of  $\mathbf{p}_U$  are implemented in scenarios (D) and (RP)

$$\begin{cases} \hat{\mathbf{p}}_U^D = \underset{\hat{\mathbf{p}}_U}{\operatorname{argmin}} Q(\hat{\mathbf{p}}_U), \\ \text{s.t. } \hat{d}_{12} - d_{12} = 0 \end{cases} \quad \text{and} \quad \begin{cases} \hat{\mathbf{p}}_U^{RP} = \underset{\hat{\mathbf{p}}_U}{\operatorname{argmin}} Q(\hat{\mathbf{p}}_U), \\ \text{s.t. } \hat{\mathbf{p}}_{21} - \exp[\hat{\theta}]_\times \mathbf{p}_{12}^r = \mathbf{0} \end{cases}$$

where  $\hat{\theta} := \operatorname{atan2}(\hat{y}_{21}, \hat{x}_{21})$  and  $Q(\mathbf{p}_U)$  is defined in (46). We evaluate the localization performance by computing the empirical MSE  $\widetilde{MSE}_{U,k} := \frac{1}{2}[\widetilde{MSE}_{1,k} + \widetilde{MSE}_{2,k}]$  for the two tag positions, using the same process as in Section VII-A2, with  $M = 500$  simulations.

TABLE I: Monte Carlo Simulation Results. Empirical MSE at the initial and terminal point, with  $3\sigma$  confidence bounds.

	$\widetilde{MSE}_{U,0}$	Confidence	$\widetilde{MSE}_{U,F}$	Confidence	ET
(D)	4.28 m <sup>2</sup>	$\pm 0.03$ m <sup>2</sup>	0.93 m <sup>2</sup>	$\pm 0.02$ m <sup>2</sup>	1.70 s
(RP)	2.97 m <sup>2</sup>	$\pm 0.04$ m <sup>2</sup>	0.63 m <sup>2</sup>	$\pm 0.002$ m <sup>2</sup>	1.89 s

The results shown in Table I indicate that the motion significantly improves the estimate accuracy in both cases: around 78% for (D) and 79% for (RP). Moreover, the relative position constraints provides a clear improvement to the MSE compared to only using the relative distance information. Table

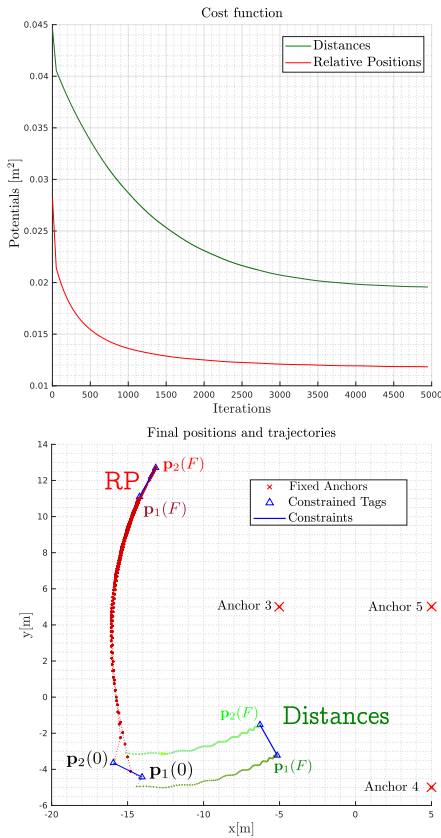


Fig. 10: Deployment results for (D) and (RP) scenarios. The cost functions are plotted as well as the positions during the trajectory.

I also provides the Execution Times (ET) of the deployment algorithms for all the steps shown in Fig. 10. The simulation is coded in Matlab R2018b and runs on a computer equipped with an Intel I7 processor. The ET for the (RP) scenario is about 10% larger than for (D), due to the increased complexity to evaluate  $\mathbf{A}$  and its derivative. In summary, compared to (D), deployment using (RP) leads to a significant improvement of the precision and a moderate increase of the ET.

## VIII. EXPERIMENTS

To validate experimentally some of the ideas presented in this paper, we placed two tags  $\mathcal{U} = \{1, 2\}$  on the *same* ground robot  $R_1$  and two anchors  $\mathcal{K} = \{3, 4\}$  on two other robots  $R_3$  and  $R_4$ , as shown on Fig. 11. The anchors are externally positioned with a motion capture system, which is also used in the following to provide the true positions of the tags and evaluate the accuracy of position estimates. The anchors and tags are based on Qorvo's DW1000 UWB modules [55]. Each tag-anchor pair  $(u, k) \in \mathcal{U} \times \mathcal{K}$  is measuring its distance  $d_{uk}$  using a bias-compensated single-sided two-way ranging protocol described in [56]. The modules are placed at known height on masts, to limit signal reflections on the ground.

Robot  $R_1$  is initially placed at location  $[-3, 0]^T$  in the world frame and is expected to follow the  $x$ -axis of that frame until reaching the neighborhood of the final location at coordinates  $[3, 0]^T$ , see Fig. 12 and 15. To do so, the robot's position

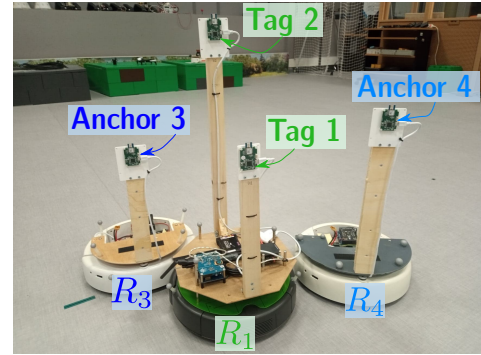


Fig. 11: Robots, anchors and tags.

is controlled by the low-level trajectory tracking controller described in Section VII-A1, using estimates  $\hat{\mathbf{p}}_{\mathcal{U}}$  of the tags' locations. These estimates are computed by collecting the four UWB-based ranging measurements  $\tilde{d}_{uk}$  between tags and anchors and solving the least-squares problem

$$\hat{\mathbf{p}}_{\mathcal{U}} = \underset{\mathbf{p}_{\mathcal{U}} \in \mathcal{C}}{\operatorname{argmin}} \sum_{k \in \mathcal{K}} \sum_{u \in \mathcal{U}} \left( \|\mathbf{p}_u - \mathbf{p}_k\| - \tilde{d}_{uk} \right)^2, \quad (47)$$

where  $\mathcal{C} := \{\operatorname{col}(\mathbf{p}_1, \mathbf{p}_2) \in \mathbb{R}^4 \mid \mathbf{p}_2 = \exp([\theta]_{\times}) \mathbf{p}_1\}$  captures constraint (37), with the relative position  $\mathbf{p}_{21}^1 = [0.3, 0]^T$  of the tags in the robot frame centered at  $\mathbf{p}_1$  known. Here  $\theta$  is the heading of  $R_1$ . Note that we do not attempt to improve the location estimates (47) by filtering them, in order to emphasize the effect of the network geometry on the localizability from the distance measurements alone.

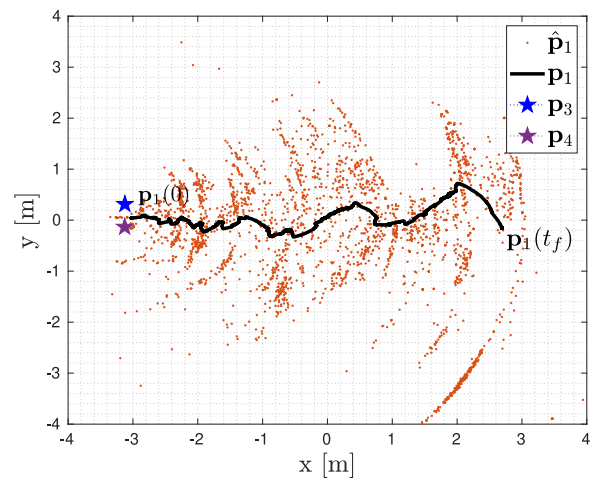


Fig. 12: Trajectory  $\mathbf{p}_1$  of tag 1 and its estimates  $\hat{\mathbf{p}}_1$  in the Cartesian plane while the anchors remain fixed.

First,  $R_1$  attempts to follow its path while the anchors remain fixed at  $[-3.3, \pm 0.3]^T$  in the Cartesian plane, as shown on Fig. 12. After each small motion,  $R_1$  stops and repeatedly computes estimates of  $\hat{\mathbf{p}}_{\mathcal{U}}$  using (47), each time using fresh measurements. The resulting estimates for tag 1 are shown by orange dots on Fig. 12. The position estimates are increasingly noisy as  $R_1$  moves toward the positive  $x$ -axis, with the  $y$ -coordinate in particular becoming increasingly



uncertain. This is intuitive because the inter-anchor distance  $d_{34}$  becomes small compared to the measured anchor-tag distances. The trajectory of the robot becomes increasingly erratic as a result of using poor estimates, which motivates improving the localizability. Although the estimates could be filtered over time to improve their accuracy and better track the desired path, this would lead to a slower system. Fig. 13 shows in blue the empirical average MSE obtained after solving (47) 500 times, together with the  $3\sigma$  confidence bounds on this MSE value. It also shows the localizability potential  $J_c$  defined in (41), which is a theoretical lower bound on the MSE. We see that  $J_c$  predicts an increasingly poor localizability as the robot moves toward the positive  $x$ -axis, which is confirmed by the empirical MSE measurements. Fig. 14 shows the squared errors  $\|\hat{\mathbf{p}}_{\mathcal{U}} - \mathbf{p}_{\mathcal{U}}\|^2$  and the potential  $J_c$  over the tags' trajectory, on a semi-logarithmic plot. We note that  $J_c$  is generally a good indicator of the order of magnitude of the expected uncertainties, which however are amplified in practice by other effects such as multipath and non-line of sight measurements [8], [10].

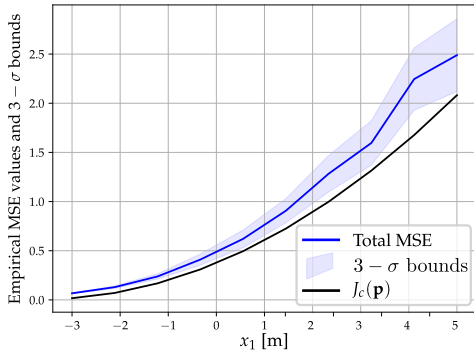


Fig. 13: Motion of robot  $R_1$  with static anchors: empirical MSE of  $\hat{\mathbf{p}}_{\mathcal{U}}$  obtained from solving (47) 500 times at each location, and localizability potential (41) for an ideal trajectory of  $R_1$  with  $y_1 = 0$ .

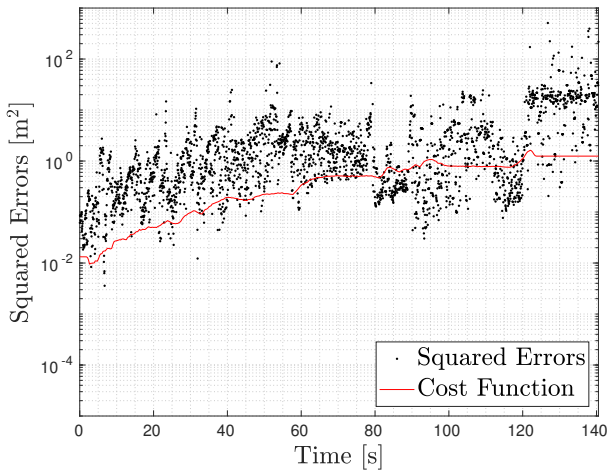


Fig. 14: Localizability potential and squared errors over the tags' trajectory, with fixed anchors.

Next, we illustrate on Fig. 15 the trajectory tracking results when the anchors are deployed simultaneously with  $R_1$ , using the gradient descent scheme described in Section VI-C, with the gradient expression (42). In this case, the position estimates produced by (47) exhibit much less variance, which is confirmed also by Fig. 16. This figure also shows that the localizability potential  $J_c$  is kept at a much lower value during the motion. The reduced variance allows us to efficiently reject measurement outliers and maintain an empirical MSE of about 12 cm along the trajectory, which is appropriate for indoor navigation. Hence, this experiment highlights that localizability can be improved automatically in real-time, even when using the position estimates to replace the true position in the gradient-based deployment algorithm.

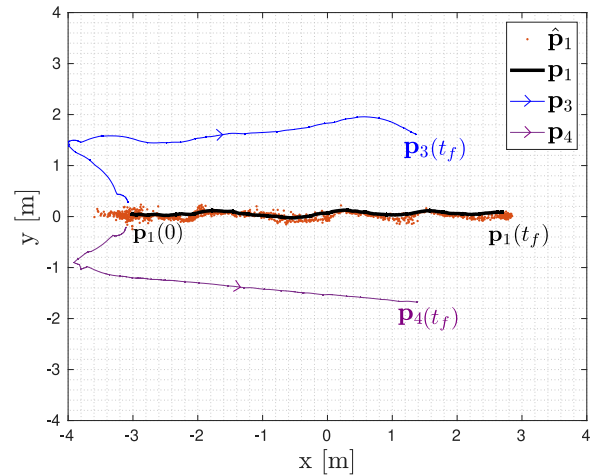


Fig. 15: Anchor and tag 1 trajectories when the anchors are mobile.

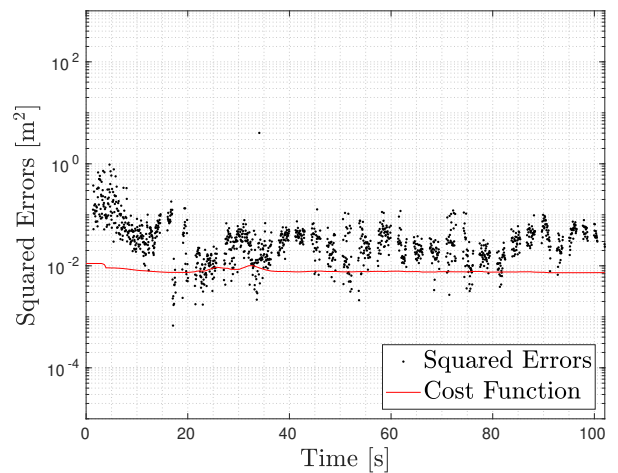


Fig. 16: Localizability and squared errors during deployment.

## IX. CONCLUSION AND PERSPECTIVES

This paper presents deployment methods applicable to Multi Robots Systems (MRS) with relative distance measure-

ments, which maximize localizability. Constrained Cramér-Rao Lower Bounds (CRLB) are used to predict the localization error of a given configuration, assuming Gaussian ranging measurement models. A connection between Fisher information matrices and rigidity matrices is highlighted, which yields useful invertibility properties, e.g., for initial MRS placement.

The CRLB is used to design artificial potentials, so that gradient descent schemes can be developed to plan robot motions that enhance the overall localizability of the network. Moreover, we show how to distribute the execution of the gradient estimation algorithms among the robots, so that they only need to communicate with their neighbors in the ranging graph. Finally, we extend the methodology to MRS with robots carrying multiple tags, again leveraging the theory of equality-constrained CRLBs. Future work could consider also optimizing the network topology, since maintaining ranging links typically entails a cost (consuming bandwidth, computation resources, etc.). Developing formal closed-loop stability properties for the gradient-based control law with noisy position estimates is also of interest.

#### ACKNOWLEDGEMENTS

The authors thank Drs. Éric Chaumette, Gaël Pagès and Ali Naouri from ISAE-Supaéro (France) for helpful discussions.

#### REFERENCES

- [1] J. Le Ny and S. Chauvière, “Localizability-constrained deployment of mobile robotic networks with noisy range measurements,” in *American Control Conference (ACC)*, Milwaukee, WI, Jun. 2018, pp. 2788–2793.
- [2] J. Cano and J. Le Ny, “Improving ranging-based location estimation with rigidity-constrained CRLB-based motion planning,” in *IEEE International Conference on Robotics and Automation (ICRA)*, Xi’an (China), 2021.
- [3] J. Sheu, W. Hu, and J. Lin, “Distributed localization scheme for mobile sensor networks,” *IEEE Transactions on Mobile Computing*, vol. 9, no. 4, pp. 516–526, Apr. 2010.
- [4] A. Prorok, A. Bahr, and A. Martinoli, “Low-cost collaborative localization for large-scale multi-robot systems,” in *IEEE International Conference on Robotics and Automation (ICRA)*, Saint Paul, MN, USA, 2012.
- [5] J. Xu, M. Ma, and C. L. Law, “AOA cooperative position localization,” in *IEEE Global Telecommunications Conference (GLOBECOM)*, New Orleans, LA, Nov. 2008.
- [6] M. Wei, R. Aragues, C. Sagues, and G. C. Calafiore, “Noisy range network localization based on distributed multidimensional scaling,” *IEEE Sensors*, vol. 15, no. 3, pp. 1872–1883, Mar. 2015.
- [7] L. Carlino, D. Jin, M. Muma, and M. Zoubir, “Robust distributed cooperative RSS-based localization for directed graphs in mixed LoS/NLoS environments,” *EURASIP Journal on Wireless Communications and Networking*, vol. 2019, Jan. 2019.
- [8] Z. Sahinoglu, S. Gezici, and I. Guvenc, *Ultra-wideband Positioning Systems: Theoretical Limits, Ranging Algorithms, and Protocols*. Cambridge: Cambridge University Press, 2008.
- [9] M. W. Mueller, M. Hamer, and R. D’Andrea, “Fusing ultra-wideband range measurements with accelerometers and rate gyroscopes for quadcopter state estimation,” in *IEEE International Conference on Robotics and Automation (ICRA)*, Seattle, WA, USA, May 2015, pp. 1730–1736.
- [10] J. Cano, S. Chidami, and J. Le Ny, “A Kalman filter-based algorithm for simultaneous time synchronization and localization in UWB networks,” in *IEEE International Conference on Robotics and Automation (ICRA)*, Montreal, QC, Canada, May 2019.
- [11] R. M. Buehrer, H. Wymeersch, and R. M. Vaghefi, “Collaborative sensor network localization: Algorithms and practical issues,” *Proceedings of the IEEE*, vol. 106, no. 6, pp. 1089–1114, 2018.
- [12] T.-S. Tay and W. Whiteley, “Generating isostatic frameworks,” *Structural Topology*, vol. 11, Jan. 1985.
- [13] K. Cao, Z. Han, X. Li, and L. Xie, “Ratio-of-Distance Rigidity Theory With Application to Similar Formation Control,” *IEEE Transactions on Automatic Control*, vol. 65, no. 6, pp. 2598–2611, Jun. 2020.
- [14] J. Aspnes, T. Eren, D. K. Goldenberg, A. S. Morse, W. Whiteley, Y. R. Yang, B. D. Anderson, and P. N. Belhumeur, “A theory of network localization,” *IEEE Transactions on Mobile Computing*, vol. 5, no. 12, pp. 1663–1678, 2006.
- [15] N. Patwari, J. N. Ash, S. Kyperountas, A. O. Hero, R. L. Moses, and N. S. Correal, “Locating the nodes: cooperative localization in wireless sensor networks,” *IEEE Signal Processing Magazine*, vol. 22, no. 4, pp. 54–69, Jul. 2005.
- [16] P. D. Groves, *Principles of GNSS, inertial, and multisensor integrated navigation systems*, 2nd ed. Artech House, 2013.
- [17] Y. Kim and M. Mesbahi, “On maximizing the second smallest eigenvalue of a state-dependent graph Laplacian,” *IEEE Transactions on Automatic Control*, vol. 51, no. 1, p. 117, 2006.
- [18] N. Michael, M. M. Zavlanos, V. Kumar, and G. J. Pappas, “Maintaining connectivity in mobile robot networks,” in *Experimental Robotics*, B. Siciliano, O. Khatib, F. Groen, O. Khatib, V. Kumar, and G. J. Pappas, Eds. Springer, 2009, vol. 54, pp. 117–126, Springer Tracts in Advanced Robotics.
- [19] P. Yang, R. Freeman, G. Gordon, K. Lynch, S. Srinivasa, and R. Suktanar, “Decentralized estimation and control of graph connectivity for mobile sensor networks,” *Automatica*, vol. 46, pp. 390–396, 2010.
- [20] I. Shames, B. Fidan, and B. D. Anderson, “Minimization of the effect of noisy measurements on localization of multi-agent autonomous formations,” *Automatica*, vol. 45, no. 4, pp. 1058–1065, 2009.
- [21] D. Zelazo, A. Franchi, P. Allgöwer, H. Bühlhoff, and P. Robuffo Giordano, “Rigidity maintenance control for multi-robot systems,” in *Robotics: Science and Systems VIII*, Jul. 2012.
- [22] D. Zelazo, A. Franchi, H. H. Bühlhoff, and P. Robuffo Giordano, “Decentralized rigidity maintenance control with range measurements for multi-robot systems,” *The International Journal of Robotics Research*, vol. 34, no. 1, pp. 105–128, Jan. 2015.
- [23] Z. Sun, C. Yu, and B. D. O. Anderson, “Distributed optimization on proximity network rigidity via robotic movements,” in *Chinese Control Conference (CCC)*, Hangzhou, China, Jul. 2015, pp. 6954–6960.
- [24] A. J. Haug, *Bayesian estimation and tracking: a practical guide*. Wiley, 2012.
- [25] H. Choset, K. Lynch, S. Hutchinson, K. George, W. Burgard, L. Kavraki, and S. Thrun, *Principles of Robot Motion*. The MIT Press, 2005.
- [26] R. McAulay and E. Hofstetter, “Barankin bounds on parameter estimation,” *IEEE Transactions on Information Theory*, vol. 17, no. 6, pp. 669–676, Nov. 1971.
- [27] D. Uciński, *Optimal measurement methods for distributed parameter system identification*. CRC press, 2004.
- [28] F. Pukelsheim, *Optimal Design of Experiments*. SIAM, 2006.
- [29] J. Le Ny and G. J. Pappas, “On trajectory optimization for active sensing in Gaussian process models,” in *IEEE Conference on Decision and Control (CDC)*, Shanghai, China, 12 2009.
- [30] H. Carrillo, I. Reid, and J. A. Castellanos, “On the comparison of uncertainty criteria for active SLAM,” in *IEEE International Conference on Robotics and Automation (ICRA)*, St Paul, MN, USA, May 2012, pp. 2080–2087.
- [31] J. D. Gorman and A. O. Hero, “Lower bounds for parametric estimation with constraints,” *IEEE Transactions on Information Theory*, vol. 36, no. 6, pp. 1285–1301, 1990.
- [32] S. Bonnabel and A. Barrau, “An intrinsic Cramér-Rao bound on lie groups,” in *Geometric Science of Information*. Springer International Publishing, 2015, pp. 664–672.
- [33] G. S. Chirikjian, “From Wirtinger to Fisher information inequalities on spheres and rotation groups,” in *IEEE International Conference on Information Fusion (FUSION)*, Cambridge, United Kingdom, Jul. 2018, pp. 730–736.
- [34] A. Bensus, *Wireless positioning technologies and applications*, 2nd ed. Artech House, 2016.
- [35] A. J. Coulson, A. G. Williamson, and R. G. Vaughan, “A statistical basis for lognormal shadowing effects in multipath fading channels,” *IEEE Transactions on Communications*, vol. 46, no. 4, pp. 494–502, Apr. 1998.
- [36] O. Khatib, “Real-time obstacle avoidance for manipulators and mobile robots,” in *Autonomous robot vehicles*. Springer, 1986, pp. 396–404.
- [37] F. Bullo, J. Cortés, and S. Martínez, *Distributed control of robotic networks: a mathematical approach to motion coordination algorithms*. Princeton University Press, 2009.

- [38] J. Cano, G. Pages, E. Chaumette, and J. Le Ny, "Optimal localizability criterion for positioning with distance-deteriorated relative measurements," in *International Conference on Intelligent Robots and Systems (IROS)*, Kyoto, Japan, October 2022.
- [39] S. M. Kay, *Fundamentals of Statistical Signal Processing: Estimation Theory*. Englewood Cliffs, NJ, USA: Prentice-Hall, 1993.
- [40] K. B. Petersen and M. S. Pedersen, "The matrix cookbook," Technical University of Denmark, Tech. Rep., 2012.
- [41] W. Whiteley, "Some matroids from discrete applied geometry," in *Contemporary Mathematics*, J. E. Bonin, J. G. Oxley, and B. Servatius, Eds. Providence, Rhode Island: American Mathematical Society, 1996, vol. 197, pp. 171–311.
- [42] C. Godsil and G. F. Royle, *Algebraic graph theory*. Springer, 2001.
- [43] D. Moore, J. Leonard, D. Rus, and S. Teller, "Robust distributed network localization with noisy range measurements," in *International Conference on Embedded Networked Sensor Systems*, Baltimore, MD, USA, 2004, p. 50–61.
- [44] D. A. Harville, *Matrix Algebra from a Statistician's Perspective*. New York, NY: Springer, 1997.
- [45] D. Bertsekas and J. Tsitsiklis, *Parallel and distributed computation: numerical methods*. Athena Scientific, 2015.
- [46] S. S. Kia, B. Van Scoy, J. Cortes, R. A. Freeman, K. M. Lynch, and S. Martinez, "Tutorial on dynamic average consensus: The problem, its applications, and the algorithms," *IEEE Control Systems Magazine*, vol. 39, no. 3, pp. 40–72, 2019.
- [47] D. P. Bertsekas, *Nonlinear programming*, 3rd ed. Belmont, MA: Athena Scientific, 2016.
- [48] T. D. Barfoot, *State estimation for robotics*. Cambridge University Press, 2017.
- [49] K. Lynch and F. Park, *Modern Robotics: Mechanics, Planning, and Control*. Cambridge University Press, 2017.
- [50] G. Gallego and A. Yezzi, "A compact formula for the derivative of a 3-D rotation in exponential coordinates," *Journal of Mathematical Imaging and Vision*, vol. 51, no. 3, pp. 378–384, Mar. 2015.
- [51] V. Mai, M. Kamel, M. Krebs, A. Schaffner, D. Meier, L. Paull, and a. R. Siegart, "Local positioning system using UWB range measurements for an unmanned blimp," *IEEE Robotics and Automation Letters*, vol. 3, no. 4, pp. 2971–2978, Oct. 2018.
- [52] A. Prorok, "Models and Algorithms for Ultra-Wideband Localization in Single- and Multi-Robot Systems," PhD Thesis, Ecole Polytechnique Fédérale de Lausanne (EPFL), 2013.
- [53] P. Corke, *Robotics, Vision and Control*, ser. Springer Tracts in Advanced Robotics, B. Siciliano and O. Khatib, Eds. Springer, 2011, vol. 73.
- [54] A. Astolfi, "Exponential stabilization of a wheeled mobile robot via discontinuous control," *Journal of Dynamic Systems, Measurement, and Control*, vol. 121, no. 1, pp. 121–126, Mar. 1999.
- [55] *DWM1000 datasheet*, Qorvo (formerly Decawave), 2022. [Online]. Available: <https://www.qorvo.com/products/p/DWM1000>
- [56] J. Cano, G. Pages, E. Chaumette, and J. Le Ny, "Clock and Power-Induced Bias Correction for UWB Time-of-Flight Measurements," *IEEE Robotics and Automation Letters*, pp. 2431–2438, 2022.